Check for updates

Antarctic Krill Biomass and Flux Measured Using Wideband Echosounders and Acoustic Doppler Current Profilers on Submerged Moorings

George R. Cutter Jr.[1]*, Christian S. Reiss[1], Sven Nylund[2] and George M. Watters[1]

[1] *Southwest Fisheries Science Center, Antarctic Ecosystem Research Division, National Oceanic and Atmospheric Administration, La Jolla, CA, United States,* [2] *Nortek Group, Nortek AS, Rud, Norway*

During austral summer 2018/2019, we deployed an array of six submerged moorings equipped with Nortek Signature100 integrated wideband echosounder and acoustic Doppler current profilers (ADCPs) on the continental shelf of the northern Antarctic Peninsula. Acoustic data from these instruments were used to classify targets, estimate water flow and the biomass of Antarctic krill (*Euphausia superba*), and quantify krill flux (biomass transport). We differentiated krill from other target aggregations using a supervised classification of data from the echosounder representing five wideband frequency bins spanning 68–113 kHz and two narrowband frequencies at 70 and 120 kHz. We estimated krill biomass using echosounder data collected at 120 kHz and water flow using the ADCP data. We estimated the biomass flux from the product of mean volumetric krill density and flow speed over a depth-integration range of 150 m. The overall mean krill areal biomass density based on hourly averages was 174 g·m^{-2} during the austral summer (December–March). Mean daily biomass decreased by an order of magnitude, from 300 to 31 g·m^{-2}, over the sampling period, and fluctuated by nearly a factor of 4 above and below the local trend within weekly intervals. Mean current direction was along-shelf toward the west, and mean flow speed increased from ∼0.10 to 0.14 m·s^{-1} during the season. Krill flux was correlated with biomass variation, and the grand mean flux was 0.13 g·m^{-2}·s^{-1}. During the study period and in our approximately 1,300 km^2 study area, average total biomass of krill was 116265 metric tons, and total cumulative krill biomass was 2.5 million tons. Our results demonstrate the utility of integrated echosounder-ADCP systems for quantifying krill flux in an important foraging area used by krill-dependent predators (seabirds and marine mammals) that breed nearby and highlight the scales of variability in a key prey resource required by these predators.

Keywords: Antarctic krill, flux, transport, biomass, Signature100, wideband echosounder, acoustic Doppler current profiler (ADCP)

INTRODUCTION

Antarctic krill (*Euphausia superba*) are abundant in the Southwest Atlantic sector of the Southern Ocean and are a critical component of the diets of seabirds (Bestley et al., 2020), fishes (Kock et al., 2012), and marine mammals (Laws, 1977; Siniff, 1991) near the South Shetland Islands. Antarctic krill are targeted by an international fishery that is managed, by the Commission for the Conservation of Antarctic Marine Living Resources (CCAMLR), with a goal of ensuring that fishing does not negatively affect populations of krill-dependent predators. Recent krill-fishing activities overlap in time and space with predators foraging for krill near the South Shetland Islands (Hinke et al., 2017), and there is empirical evidence that concentrated krill fishing has impacted seabirds (Krüger et al., 2020; Watters et al., 2020). Some of the evidence for such impacts hinges on time-series estimates of krill biomass.

Like other surveys of euphausiids (e.g., Ressler et al., 2012; Jech et al., 2017, 2018), the biomass of Antarctic krill has been estimated using ship-borne scientific echosounders, typically as part of annual acoustic surveys that include net sampling (e.g., Reiss et al., 2008; Fielding et al., 2014). These surveys lack temporal detail; they usually aim to cover the spatial area of the population of interest in the shortest possible time. With dedicated efforts and resources, annual surveys of this nature supply resource managers with biomass indices relevant to relatively broad spatial scales and annual time scales (e.g., regional or stratum-specific estimates of krill biomass during January of each year), but they do not provide data on the time varying nature of the target population between episodic sampling periods. Quantifying temporal variations in the abundance of krill and other forage species more frequently than once or twice a year may provide new insights into predator breeding and foraging success, be useful for developing indices to support ecosystem-based fishery management, or aid interpretation of trends in fishery catches and effort. There is a need to develop sampling approaches that can capture the time varying nature of fished species in high resolution.

Because of the high cost of increasing the number of scientific surveys to cover expanded fishing seasons and ecosystem-based management approaches, combined with the need to better understand the relationship between krill availability, predator foraging, and fishing, a number of solutions have been proposed to increase the temporal coverage of data collection. One approach is to outfit fishing vessels with calibrated echosounders that then survey the fishing grounds for the duration of the fishing season (Godø et al., 2014; Watkins et al., 2016). Such surveys could fit into more general observation programs (e.g., Handegard et al., 2012) but are not fishery-independent. Alternatively, autonomous instruments could be used to monitor the ecosystem (Greene et al., 2014; Rudnick, 2016; Testor et al., 2019) or conduct fisheries surveys (Mordy et al., 2017; Meinig et al., 2019). In the Antarctic, Reiss et al. (2021) have shown that buoyancy-driven gliders equipped with echosounders provide estimates of krill density in proximity to predator colonies. Another cost-effective alternative to long-period ship surveys is to use moored acoustic instruments ("acoustic moorings") to observe biological and physical phenomena.

Moored and ship-based acoustic Doppler current profilers (ADCPs) have proven effective for documenting spatial and temporal patterns of krill at a range of spatial scales (Zhou et al., 1994; Zhou and Dorland, 2004; Tarling and Thorpe, 2014). For example, Murphy et al. (2004) estimated krill flux along a ship transect based on echosounder, ADCP, and hydrographic data. Brierley et al. (2006) used an ADCP and a separate echosounder on a single mooring to describe the time varying flux of acoustic backscatter attributed to krill near South Georgia, an important krill-fishing area. More generally, biomass estimates from a moored acoustic array may be comparable to those from a ship-based survey, at least during periods when the two overlap (De Robertis et al., 2018). Acoustic moorings equipped with ADCPs and echosounders (e.g., Lee et al., 2004; Brierley et al., 2006) may provide a scalable solution to understanding the time varying nature of krill density. Recent development of an ADCP with an integrated wideband echosounder (Velasco et al., 2018) provides the ability to simultaneously discriminate acoustic target types (via differences between echosounder returns at various frequencies) and quantify their advection through the water using the flow data.

Here we examine the time varying biomass of Antarctic krill over the continental shelf near an important colony of krill predators breeding on Livingston Island, Antarctica, in the same area that Reiss et al. (2021) surveyed using gliders. We use an array of six upward looking 100 kHz ADCPs with integrated wideband (68–120 kHz) echosounders (Velasco et al., 2018) to quantify the flux of krill through the predators' foraging area during December 2018 – March 2019. We implement a supervised method to classify acoustic scatterers as krill, "fish" (fish without swim bladders, squid, or similar), and other types using the volume backscattering strength data from seven frequency bins sampled by the echosounder, and we estimate the biomass density ($g \cdot m^{-2}$), total biomass (t), and flux ($g \cdot m^{-2} \cdot s^{-1}$) of krill. We discuss the results of the biomass estimates in relation to other surveys and the needs of predators and the fishery.

MATERIALS AND METHODS

Study Area and Mooring Array

Our study area occurs over the continental shelf offshore of Cape Shirreff, Livingston Island, Antarctica (**Figure 1**). This area is an important foraging ground for birds and mammals breeding at Cape Shirreff during the austral summer (Hinke et al., 2017). Several bathymetric features in the study area likely affect the distribution of krill. The gently sloping continental shelf off Cape Shirreff is relatively narrow and is intersected by two canyons, one on either side of the Cape. The canyons are about 400–500 m deep, 30 km long, and 2–10 km wide. The canyons open at the continental slope, into waters that deepen to 5000 m in the nearby South Shetland Trough. The canyons have sills that may affect flows in and out (**Figure 1**).

Six subsurface moorings were deployed by the U.S. Antarctic Marine Living Resources (AMLR) Program, during cruise LMG 18-11 aboard the Antarctic Research and Supply Vessel *Laurence*
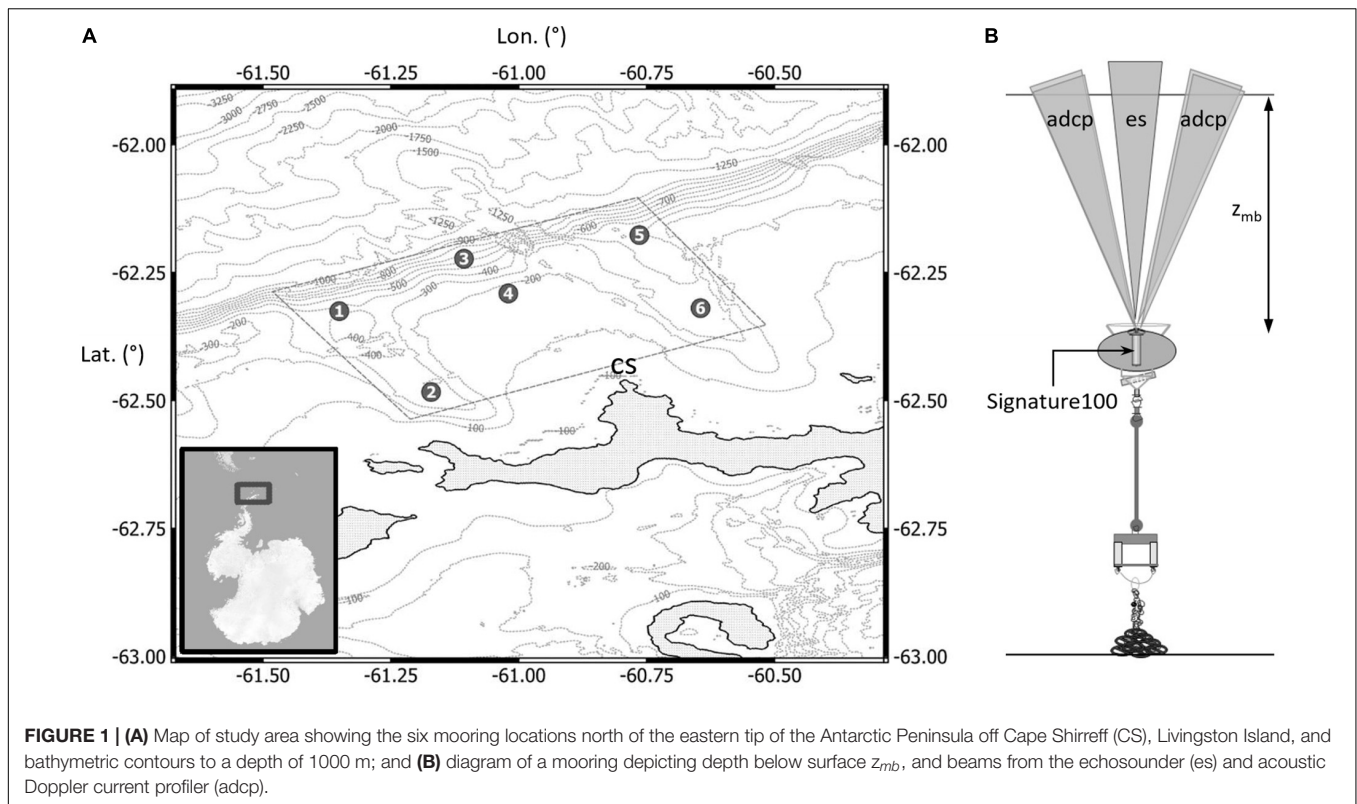
FIGURE 1 | (A) Map of study area showing the six mooring locations north of the eastern tip of the Antarctic Peninsula off Cape Shirreff (CS), Livingston Island, and bathymetric contours to a depth of 1000 m; and **(B)** diagram of a mooring depicting depth below surface z_{mb}, and beams from the echosounder (es) and acoustic Doppler current profiler (adcp).

TABLE 1 | Location, water depth, and buoy depths for U.S. AMLR moorings deployed during the Antarctic summer 2018–2019.

Mooring	Latitude	Longitude	Nominal depth (m)	Line (m)	Nominal depth of buoy (m)
1	62° 19.52′ S	61° 21.05′ W	400	50	350
2	62° 29.00′ S	61° 10.27′ W	400	50	350
3	62° 13.38′ S	61° 06.41′ W	700	350	350
4	62° 17.44′ S	61° 01.22′ W	175	10	165
5	62° 10.59′ S	60° 45.84′ W	400	50	350
6	62° 19.16′ S	60° 38.67′ W	400	50	350

M. Gould, in an array offshore of Cape Shirreff. The moorings were deployed between 10 and 12 December 2018 and recorded data beginning at 00:00 UTC on 15 December 2018. The instruments continued collecting data until their storage devices were full on about 3 March 2019, and the moorings were recovered soon thereafter. The six moorings were deployed in an array such that they sampled nearshore and offshore locations within the two canyons and on the continental shelf between the canyons. We attempted to minimize the risk of losing moorings from iceberg scour. Five of the six moorings had buoys at 350 m below the water surface, but the buoy for the shallowest mooring was located at about 165 m. The four canyon moorings were deployed at 400 m, with 50 m of line between the sea floor and the buoy. The deepest mooring was located on the edge of the shelf in 750 m of water with 350 m of line, and the shallowest mooring was in ~175 m water depth with 10 m of line (**Figure 1A** and **Table 1**).

During the deployment, the presence of sea-ice and icebergs, which could significantly impact the biomass estimates, were monitored as part of another study (Reiss et al., 2021). With the exception of two large, grounded icebergs, there was little if any seasonal sea-ice or icebergs in this region during the study period.

Moorings

Each mooring consisted of a 1.12-m diameter, elliptical ADCP buoy (DeepWater Buoyancy Inc., Biddeford, ME, United States) made from syntactic foam; a swivel; and a line (12-strand single braid, non-rotational rope, 5/16″ diameter with 8,600-lb average tensile strength with plastic thimbles) attached to dual acoustic releases (Edgetech PORT LF Push Off Release Transponder) ballasted by 255–380 kg of steel weight (**Figure 1B**). The ballast was connected to a 5-m length of chain shackled to an oblong link through which additional chain joining the two acoustic releases passed. All mooring buoys were also equipped with an LED flasher and Iridium beacon (XMF-11K & XMI-11K from Xeos Technologies Inc., Dartmouth, NS, Canada) to facilitate tracking in case of early separation from the ballast.

Each mooring was equipped with a single Nortek Signature100 ADCP with an integrated wideband (68–120 kHz) scientific echosounder (Firmware version 2208_0). The Signature100 was installed into a cavity in the center of each mooring buoy, and oriented with transducers facing upward toward the water surface (**Figure 1B**). The Signature100 units operate in both wideband (68–113 kHz) and narrowband (70 and 120 kHz) modes, and the sequence of transmission and receive cycles ("pings") begins with the ADCP ping, followed by the wideband echosounder ping, and then the 70 and 120 kHz narrowband echosounder pings.

Acoustic Doppler Current Profilers Operation and Data Processing

The ADCPs operated at a center frequency of 100 kHz and acquired samples at an interval of 6 s over an averaging period of 240 s, a burst interval of 600 s, a transmit power level of –6 dB, and a range bin size of 10 m. Data from each 6-s interval and 240-s averaging period were recorded to an internal storage device in .ad2cp format. Orientation data were recorded by the internal attitude and heading reference sensors, which measured magnetic compass heading and tilt (Velasco et al., 2018). Compass heading values were adjusted by the magnetic declination for the study area (12.1°), based on the World Magnetic Model of 2015[1]. The Signature100 is also equipped with a thermometer and pressure sensor to measure temperature at and determine the depth of the instrument when sampling. Velocity data from the ADCP were recorded relative to north-south, east-west, and up-down axes given the internal, calibrated, magnetic compass heading.

Echosounder Operation

The Signature100 echosounders were operated to transmit and receive a sequence of one wideband and two narrowband pulses, all using the maximum transmit power level (0 dB). ADCP and echosounder pings were sequential and separated by a 1-s delay to allow time for two-way sound propagation and signal processing. All echosounder operational modes use the same transducer. Ping 1 comprised a linear chirp signal pulse spanning 68–113 kHz with a 5-ms pulse duration. The transmit pulse signal was recorded with the data. The echo pressure amplitude signal from the wideband ping was converted by the internal processor into an echogram representing received power in five frequency bins (Velasco et al., 2018). Ping 2 was a narrowband (monochromatic wave, MW) pulse transmitted at 70 kHz with a 1-ms duration, and Ping 3 was a narrowband pulse at 120 kHz with 1-ms duration. The echosounders sampled to a range of 400 m, and binned data were stored using the minimum available range bin size of 0.375 m for both narrow- and frequency-binned wideband modes. Frequency-binned echograms were recorded to internal storage for every ping in Nortek's .ad2cp file format.

In addition to the frequency-binned data stored for each channel, the digitized, raw, quadrature-sampled, complex time series (I-Q) data representing the received demodulated, received signal from the wideband echosounder were recorded at a sample rate of 45454 Hz every 30 s. The longer interval for recording raw data was chosen based on available storage

capacity relative to our prioritized short ping interval and 3-month deployment. For processing, the .ad2cp files were converted to MATLAB format (.mat) using Nortek's Signature Deployment software, version 3.4.17.0. Data in the .mat files were processed using MATLAB code developed by the authors and available by request. Alternatively, commercial software applications are now incorporating the ability to read and process Signature100 data files.

Target Strength and Volume Backscattering Strength

Target strength (TS; dB re 1 m^2) and volume backscattering strength (S_v; dB re 1 m^{-1}) were obtained from the Signature100 data by converting the recorded squared amplitude (P, dB) values that result from internal processing of the raw data.

Our solutions for TS, S_v and calibration gain for the Signature100 echosounder are equivalent to the formulations of Cochrane et al. (2003) and principally based on their equations 1, 9, and 12. The power values P recorded by the Signature100 can be related to the transmit-to-receive power term of Cochrane et al. (2003).

TS and S_v are computed using the following relationships:

$$TS_u = P + 40\log_{10}r + 2\alpha r + G_{PL}$$

$$S_{vu} = P + 20\log_{10}rr + 2\alpha r - 10\log_{10}\Psi$$

$$-10\log_{10}\left(\frac{c\tau}{2}\right) + G_{PL}$$

where r is range (m); α is absorption (dB·m^{-1}); τ is the pulse duration (s); $P = 20\log_{10}(p_{rec})$; and p_{rec} is the received amplitude. The subscript u indicates that the TS and S_v values are uncalibrated at this stage of processing. For S_v from wideband data, the effective pulse duration was obtained by dividing τ by the number of frequency bins (5) because they were equal in bandwidth. G_{PL} represents the Signature100 transmit power level that can be set by the operator in the range from 0 dB to –12 dB. For our deployment $G_{PL} = 0$.

Ψ is the equivalent beam angle modeled for a piston transducer (Clay and Medwin, 1977) with active radius $a = 0.0435$ m;

$$\Psi = \left(\frac{5.78}{(ka)^2}\right)$$

(Amakasu et al., 2017). $k = 2\pi/\lambda$ (cycles·m^{-1}) is the wavenumber magnitude; $\lambda = c/f$ (m) is wavelength; c (m·s^{-1}) is sound speed; and f (Hz, or cycles·s^{-1}) is frequency.

The frequency-dependent absorption α (**Table 2**) was modeled following Kinsler et al. (1999), where the average sound speed for water in the survey area and period was approximately $c = 1450$ m·s^{-1}, based on the mean temperature ($T = 0.5°$) and salinity ($S = 34$ psu) in our study area.

Cochrane et al. (2003) provide expressions for TS and S_v that include a term representing the ratio of received to transmit power, $20\log_{10}(p_{rec}/p_{xmit})$. We explicitly use only received power from the Signature100 for computing the uncalibrated S_v; the transmit power is implicitly accounted for by the calibration gain.

Echosounder Calibration

Prior to deployment, the Signature100 echosounders were calibrated on-axis using a 25.4-mm diameter tungsten carbide sphere (Foote et al., 1987; Cochrane et al., 2003; Atkins et al., 2008; Perrot et al., 2014; Demer et al., 2015a; Lunde and Korneliussen, 2016; Amakasu et al., 2017) in a seawater tank at the Southwest Fisheries Science Center (Demer et al., 2015b). The sphere was positioned at a range of approximately 4–4.5 m from the transducer, ensuring far-field ensonification at the largest range possible before the tank walls were detected by the beam sidelobes. Following Atkins et al. (2008) and Amakasu et al. (2017) echo strength values below the 90th percentile value were discarded, assuming that the lower values were from off-axis target positions. For calibration, raw IQ data were stored for every transmit and receive cycle at a 6-s interval.

Calibration gain offset values C_{cal} for each echosounder and channel were computed as differences between the measured TS and theoretical TS of the standard sphere, $C_{cal} = TS_{theor} - TS_{meas}$, and were used to compute calibrated TS and S_v by adding C_{cal} to the uncalibrated values:

$$TS_{cal} = TS_u + C_{cal}$$

$$S_{vcal} = S_{vu} + C_{cal}$$

The calibration gain term C_{cal} represents an offset equivalent to that in equations 9 and 12 of Cochrane et al. (2003).

Wideband Data Frequency-Bins

We recorded wideband echosounder data in five frequency bins representing bands around center frequencies $f_{c(FM)} =$ 74, 82, 91, 99, and 108 kHz with bandwidth $bw_{(FM)} = 9$ kHz, and narrowband data in two frequency bins at $f_{c(CW)} = 70.0$ and 120.0 kHz with $bw_{(CW)} = 1$ kHz. TS, S_v, and C_{cal} were computed with respect to the same frequency bins, therefore $TS(f)$ and $S_v(f)$ represent TS and S_v values averaged in the linear domain over the seven bands combined as $f_c = \{f_{c(FM)}, f_{c(CW)}\}$ (**Table 2**).

Noise Removal

Noise, commonly described as "background noise" (De Robertis and Higgenbottom, 2007) and characterized by a range-dependent noise curve $N = 20 \log_{10} r + 2\alpha r + N_0$ was subtracted and removed along with S_v values with a signal-to-noise ratio

SNR < 10 dB above N. N_0 varies by frequency and mean $N_0(f)$ was approximately –126 dB.

Krill Length and Weight

The mean lengths of krill sampled from the diets of seabirds and marine mammals covary with those of krill sampled from net tows (Reid et al., 1999; Miller and Trivelpiece, 2007) and can be used to estimate the target strength of krill in the survey area (Reid and Brierley, 2001), especially when large individuals are common. For this study, krill length-frequency distributions were calculated from penguin diets sampled at Cape Shirreff (Hinke et al., 2017). Length-frequency distributions were constructed from the combined diets of five Gentoo and five chinstrap penguins sampled between 3 and 31 January 2019. Krill mass, commonly called weight, w (g), was modeled as a power function;

$$w = 2.236 \times 10^{-6} L^{3.314}$$

with length, L (mm), were measured from the anterior edge of the eye to the tip of the telson (Hewitt et al., 2004). Weighted mean mass $\langle w \rangle$ is obtained from the mass values w weighted by the proportional representation of each length within the length-frequency distribution $[p(L); \sum p(L) = 1]$.

$$\langle w \rangle = \sum_{L=10}^{L=65} w(L) \times p(L)$$

Krill lengths from our penguin diet samples ranged from 21 to 62 mm. The length-frequency distribution was unimodal; the weighted mean krill length was 46.8 mm ($SD = 6.0$ mm); and the weighted mean krill mass was 0.8 g ($SD = 0.1$ g).

Modeled Target Strength of Krill

Target strength of krill was modeled using the distorted wave Born approximation (DWBA) model (Jech et al., 2015), as implemented by Lawson et al. (2006b) and following Jech et al. (2018). We parameterized the DWBA model, using values described here and provided in **Table 3**, by modeling the backscattering cross section σ_{bs} (MacLennan et al., 2002) within each frequency band, and averaging, in the linear domain, over the assumed distribution of krill orientation (tilt) angles, $\phi_{krill} \sim N(0, 30)$ and assuming model symmetry for the actual 180° incidence of the upward echosounder. σ_{bs} was weighted by

TABLE 2 | Signature100 operational settings used during the 2018–2019 Antarctic summer deployment.

Operation mode	Echogram (order)	Freq. bin	f_c (kHz)	Band width (kHz)	Pulse duration (ms)	Absorption (dB/km)
FM/PC	1	1	73.86	9	5	18.201
FM/PC	1	2	82.38	9	5	19.698
FM/PC	1	3	90.90	9	5	20.950
FM/PC	1	4	99.43	9	5	22.309
FM/PC	1	5	107.95	9	5	23.497
MW	2	1	70.00	1	1	17.671
MW	3	1	120.00	1	1	25.436

Operation mode: FM, frequency-modulated; PC, pulse-compressed, wideband; MW, monochromatic wave, narrowband; Freq., frequency; f_c, center frequency.

TABLE 3 | Parameters used for the DWBA model of krill target strength (TS).

Parameter	Value	Units
Mean krill length <L>	46.8	(mm)
Standard deviation. of length SD(L)	4.7	(mm)
Mean krill mass <W>	0.758	(g)
Standard deviation of mass SD(W)	0.3	(g)
Density contrast	1.04	
Sound speed contrast	1.03	
Sound speed	1480	(m/s)
Orientation distribution	N(0,30)	(°)
$\langle \sigma_{bs} \rangle$ (120 khz)	7.401e-08	(m^2)
$< TS >$ (120 khz)	−71.3	(dB re 1 m^2)

Lengths are from 2018 to 2019 predator diet measurements, and weights and TS are based on models from SC-CCAMLR-XIX (Annex 4, Appendix G, p222). The length distribution was simulated using the mean and standard deviation of observed lengths.

the proportional representation of each length in the length-frequency distribution to give angle-averaged, length-weighted values $\langle \sigma_{bs} \rangle$ (m^2) (**Figure 2**). $\langle \sigma_{bs} \rangle$ was then converted to the log domain giving $\langle TS \rangle = 10 \ log_{10} \langle \sigma_{bs} \rangle$ (dB re 1 m^2) (MacLennan et al., 2002). We used a mean tilt angle of 0° because, in combination, the many previous attempts to resolve krill orientations by field observations (e.g., Lawson et al., 2006a; Cutter et al., 2009) or inversion of acoustic data (Martin-Traykovski et al., 1998) suggest that krill may orient with any angle. Krill behaviors affect each individual's orientation, and there is no strong basis for generalization, leading recent workers to assume zero mean tilt (Wiebe et al., 2011; Jech et al., 2018). Furthermore, averaging σ_{bs} over the wide tilt-angle distribution used here, where the standard deviation of tilt angles was 30°, results in a $\langle \sigma_{bs} \rangle$ value that is nearly the same as that resulting from averaging using a small but non-zero mean angle.

Acoustic Data Classification

We implemented a supervised classification of the Signature100 echosounder data to separate krill from other targets so the latter could be excluded from estimates of krill biomass. Aggregations of relatively weakly scattering targets that we believed to be animals without gas-filled swim bladders, possibly icefish (Fallon et al., 2016), myctophids, squid, salps, other small planktonic animals, or some combination of those were recorded in the echograms (**Figure 3**). Usually, these other targets occurred at greater depths, but occasionally they occurred in the depth range occupied by krill and within integration depth range limits.

Multi-frequency classification methods based on differences of mean S_v between two or three frequencies are commonly employed to classify krill (Hewitt et al., 2003; Lawson et al., 2008; Reiss et al., 2008; Fielding et al., 2014). Although the Signature100 echosounder records data in multiple frequency bands, the differences of mean S_v for krill among those bands are small, theoretically from nearly 0 dB to ~2 or 3 dB depending on the sizes and orientations, and perhaps insufficient for reliable discrimination given the usually wide distributions of S_v from krill swarms. Conceptually following classification methods based on multiple frequencies (e.g.,

Kang et al., 2002; De Robertis et al., 2010; Woillez et al., 2012; Jech et al., 2017, 2018; Kitamura et al., 2017), we implemented a supervised classification of targets identified in the wideband echosounder data using minimum L2-norm (Euclidean) distances between features defined by median S_v ($\langle S_v \rangle$) and differences of S_v (dS_v) from the five wideband and two narrowband frequency bins. We calculated a set of data-feature vectors representing $\langle S_v \rangle$ and dS_v within analyst-defined regions from a training dataset collected by Mooring 4 (**Figure 3**). These training features were accumulated from regions representing "krill," "fish, squid, or salps" usually in deep water and possibly icefish (Fallon et al., 2016), a "midwater layer" with weak and maybe small scatterers, "other (mixed or unknown)" target types, and "clear water" regions evident from visual inspection of the data (**Figure 3**). Training sample regions covered various time and depth ranges to include the features visually identified to represent each class individually.

The classification feature vectors (C_{feat}) include 18 values, where 11 of those are the median dS_v between each wideband frequency bin and all lower frequency bins, and seven are means (linear domain) of S_v for all bins. For example, $C_{feat} = [dS_{v,5-1},$ $dS_{v,5-2},$ $dS_{v,5-3},$ $dS_{v,5-4},$ $dS_{v,4-1},$ $dS_{v,4-2},$ $dS_{v,4-3},$ $dS_{v,3-1},$ $dS_{v,3-2},$ $dS_{v,2-1},$ $dS_{v,7-6},$ $\langle S_{v,1} \rangle,$ $\langle S_{v,2} \rangle,$ $\langle S_{v,3} \rangle,$ $\langle S_{v,4} \rangle,$ $\langle S_{v,5} \rangle,$ $\langle S_{v,6} \rangle,$ $\langle S_{v,7} \rangle]$, where, for example $dS_{v,5-1}$ indicates the difference of median S_v from frequency bins 5 and 1 (respectively centered at 108 and 74 kHz) of the wideband echosounder. Assignment of S_v data from other than the training set to classes was based on data from non-overlapping time-range blocks and the training class centroids. The classification sample blocks (neighborhoods) were 1 min in time (10 time intervals) and 10.125 m in range (27 range intervals) (e.g., **Figure 4**). The nearest class was assigned to all samples of each classification neighborhood; there were no partial neighborhood assignments. When the minimum Euclidean distance indicated "other/mixed" class but the distance to "krill" or "fish/squid/salp" was also small (<2), the cell was reassigned to either "krill-like" or "fish-like," based on whichever was closer. When all distances were within a threshold value (2) of each other, then the class was reassigned to "indeterminate." Including the classes occurring from reassignments, the seven classes were named: "clear," "krill," "krill-like," "fish," "fish-like," "other," and "indeterminate." "Clear" indicated regions of apparently clear water with few, if any, scatterers (**Figure 3**). The "krill-like" and "fish-like" classes were respectively combined into the "krill" and "fish" classes for the final classification based on five classes. Binary data masks were generated to allow only data from the final "krill" class to pass for further analysis. To evaluate our classification results, we compared them to original echograms visually (e.g., Jech, 2011) and considered how well the classification results represented what would have resulted from delineations based on visual scrutinization; this is a simple process that easily identifies systematic errors of classification.

Krill Biomass

Mean volume backscattering coefficient s_v (m$^2 \cdot$m^{-3}, or m^{-1}) was obtained by converting S_v to the linear domain, such that $s_v = 10^{(S_v/10)}$ for every range sample. Area backscattering coefficient values s_a (m$^2 \cdot$m^{-2}) were obtained by integrating s_v (MacLennan et al., 2002) over a depth range of 15 – 165 m. The limit
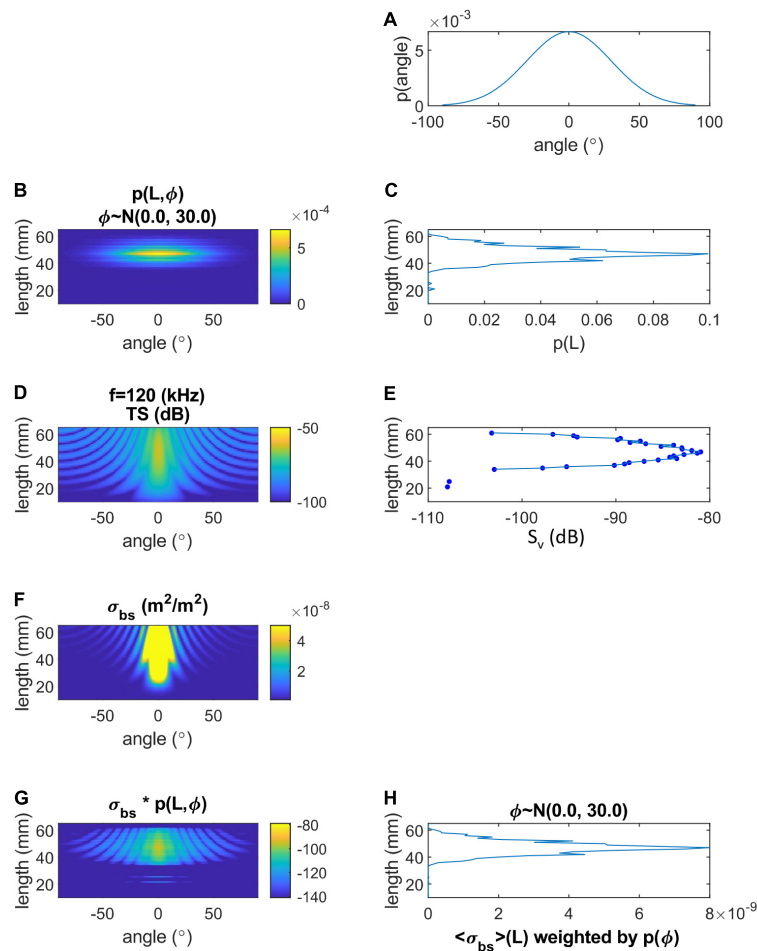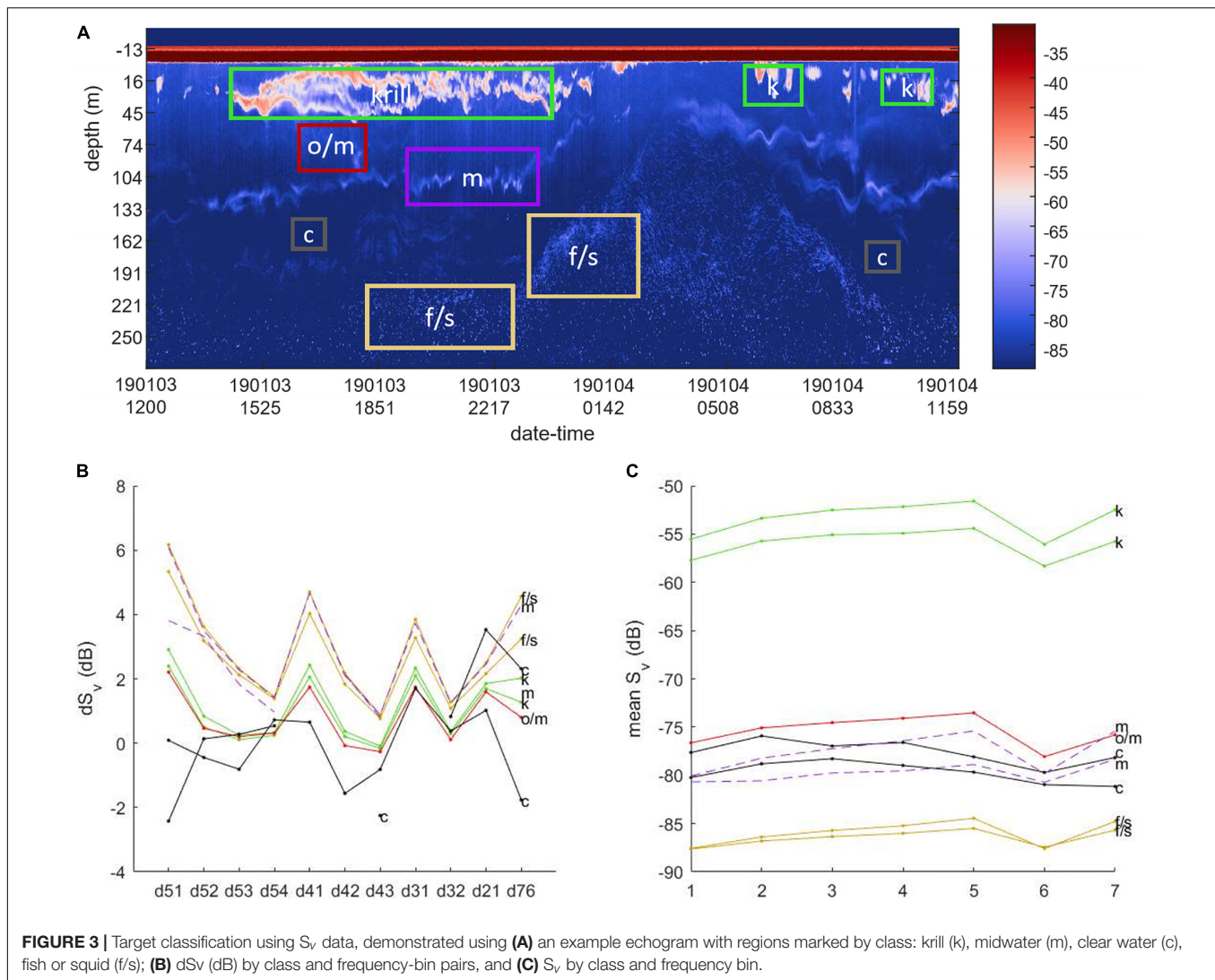
FIGURE 2 | Acoustic target strength (TS; dB) and backscattering cross section (σ_{bs}; m^2) of krill versus tilt angle (φ; °) and length (L; mm), predicted by the DWBA model. **(A)** Tilt angle distribution, **(B)** joint distribution of tilt angle and length distribution, **(C)** length distribution of krill, **(D)** DWBA-modeled TS by tilt angle and length for 120 kHz, **(E)** mean S_v by length after weighting by angle distribution, **(F)** σ_{bs} versus angle and length, **(G)** product of σ_{bs} and p(L,φ) versus angle and length, and **(H)** σ_{bs} weighted by angle distribution versus L.

of 15-m from the surface represents the typical depth that is used to exclude near-surface echosounder data from analysis for ship-based surveys (Reiss et al., 2008), and, as intended, is generally deep enough to remove surface-related echoes and features that could impact biomass estimates (e.g., the air-water interface, bubbles, and shallow surface dives by predators). To address concerns that a significant biomass of krill occurs at depths < 15 m we also estimated mean biomass density within the 10–15 m depth range for two moorings (#2 and #5) for comparison with biomass estimated from the 15–165 m depth range during daytime and nighttime. The 10 – 15 m depth range was used to represent the near-surface zone because, based on visual inspection of the full-series S_v echograms, it was usually free of obvious surface-related echo effects, such as interface echoes when waves were large and associated near surface bubbles that were frequent and sometimes dominant in depths less than 10 m. As the 10–15 m depth range was not totally free of apparent surface contamination, the estimates from this region are probably biased high. The 165-m maximum

depth limit represents the depth of the shallowest mooring (**Figure 1**) and encompassed the deepest diel vertical migration depths we observed for krill among our moorings. Krill areal density, ρ_a (no.·m^{-2}), was estimated using the integrated s_a values scaled by the length-weighted differential backscattering cross-section of krill $\langle\sigma_{bs}\rangle$ (m^2) where, $\rho_a = \frac{s_a}{\langle\sigma_{bs}\rangle}$ (MacLennan et al., 2002; Jech et al., 2018). Areal biomass density ρ_w (g·m^{-2}) is obtained by scaling krill areal density by the length-weighted mean mass $\rho_w = \rho_a\langle w\rangle$ and was estimated for each time sample. We distinguish integrated areal biomass density $\rho_{w,a}$ (g·m^{-2}) from volumetric biomass density $\rho_{w,v}$ (g·m^{-3}); the latter is used to calculate krill flux. Total biomass B (g) is obtained by extrapolation of $\rho_{w,a}$ to the full survey area $B = \rho_{w,a}A$ where $A = 1300$ km^2.

Flow

Flow velocity data arrays from the ADCP were resampled in the range direction using one-dimensional linear interpolation

FIGURE 3 | Target classification using S_v data, demonstrated using **(A)** an example echogram with regions marked by class: krill (k), midwater (m), clear water (c), fish or squid (f/s); **(B)** dS_v (dB) by class and frequency-bin pairs, and **(C)** S_v by class and frequency bin.
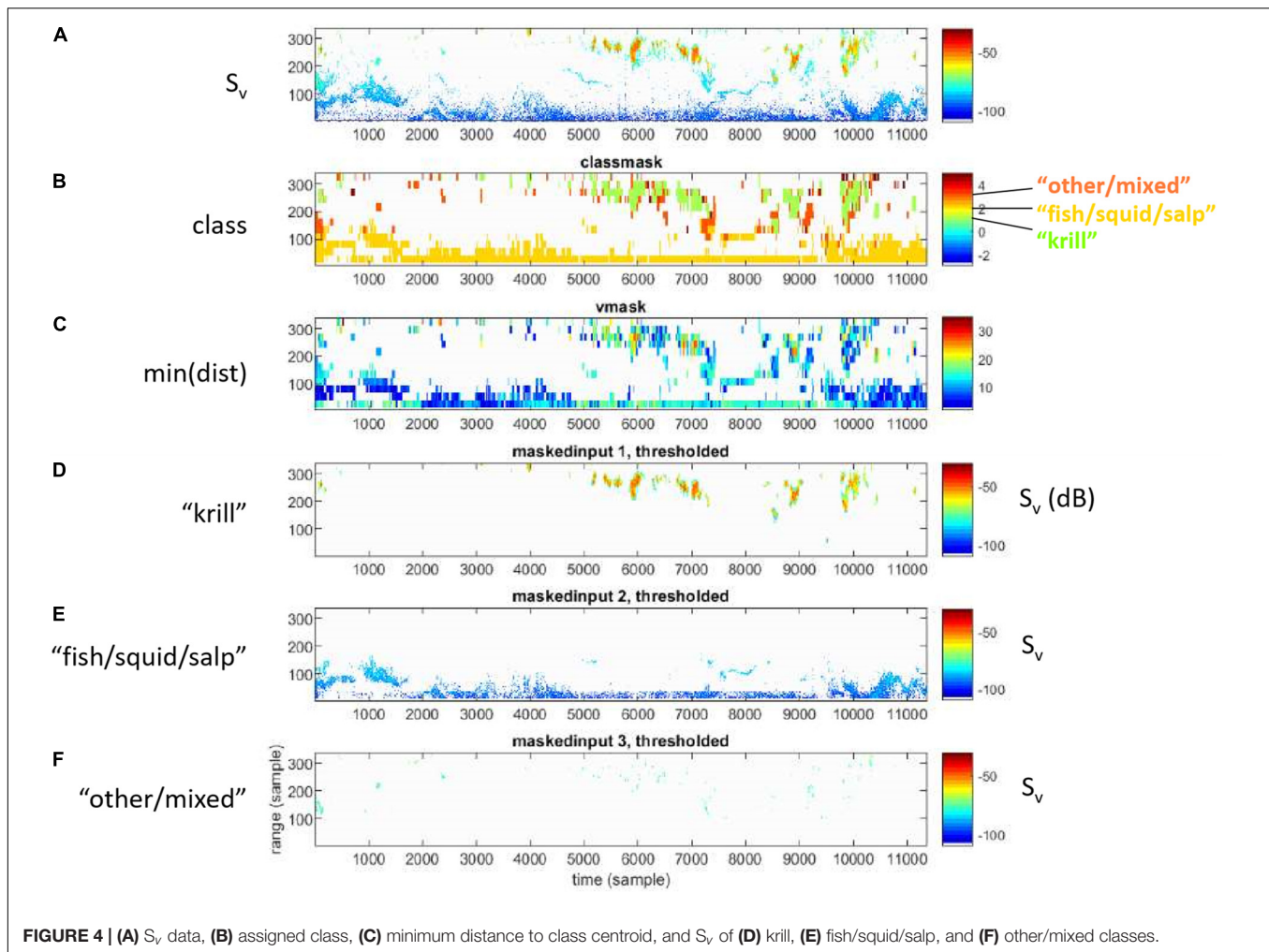
to make the ADCP data arrays the same size as those from the echosounders. This facilitated element-wise computations for flux calculations. ADCP data with mean correlations over all beams < 0.5 were converted to NaN values and did not contribute to our results. For the deep moorings, the flow data were generally highly uncorrelated from the surface to nearly 40 m because of interference caused by beam sidelobes encountering the air-water interface (Nortek, 2021). Therefore, north-south and east-west velocities (u_{N-S} and u_{E-W} respectively) from range cells spanning depths from 40 to 165 m, to match the biomass integration range as close as possible, were used to summarize flow for flux calculations. u_{N-S} and u_{E-W} data were converted to flow magnitude $|u| = \sqrt{u_{N-S}^2 + u_{E-W}^2}$ and compass direction $\emptyset_u = -1 * arctan\left(\frac{u_{N-S}}{u_{E-W}}\right) - 90° + D_{mag}$ using the four-quadrant inverse tangent that was then adjusted by the declination D_{mag}. Mean flow magnitude $\langle|u|\rangle$ was calculated for ensembles matching the hourly and daily analysis periods of the echosounder data. The pressure and temperature data from the sensors built into the

ADCP were used to characterize the tidal and lunar cycles plus changes in water temperature during the deployment period.

Krill Flux

Biomass flux, $F = \langle\rho_{w,v}\rangle <|u|>$ (g·m^{-2}·s^{-1}), was computed from the product of the mean volumetric biomass density $\langle\rho_{w,v}\rangle$ (g·m^{-3}) and the mean flow speed $<|u|>$ (m·s^{-1}) (calculated from the moored Signature100's ADCP flow data), where $\langle\rho_{w,v}\rangle$ was obtained from the quotient of the vertically integrated density estimate $\rho_{w,a}$ and the integration depth range (150 m). Instantaneous F was computed for each time sample during the averaging period of the ADCP when velocity measurements were available using each of the 6-s interval velocity samples from the 240-s ADCP averaging period.

Total biomass transport (t·s^{-1}) was computed by scaling the unit flux (based on means of biomass density and flow speed among all moorings) by the cross-sectional area of a vertical plane defined by the nominal distance across the study area from nearshore to shelf edge (20 km), and the vertical integration

FIGURE 4 | **(A)** S_v data, **(B)** assigned class, **(C)** minimum distance to class centroid, and S_v of **(D)** krill, **(E)** fish/squid/salp, and **(F)** other/mixed classes.

range (150 m). Total, cumulative biomass (t) was computed by integrating daily mean of total flux over the full survey period, 79 days.
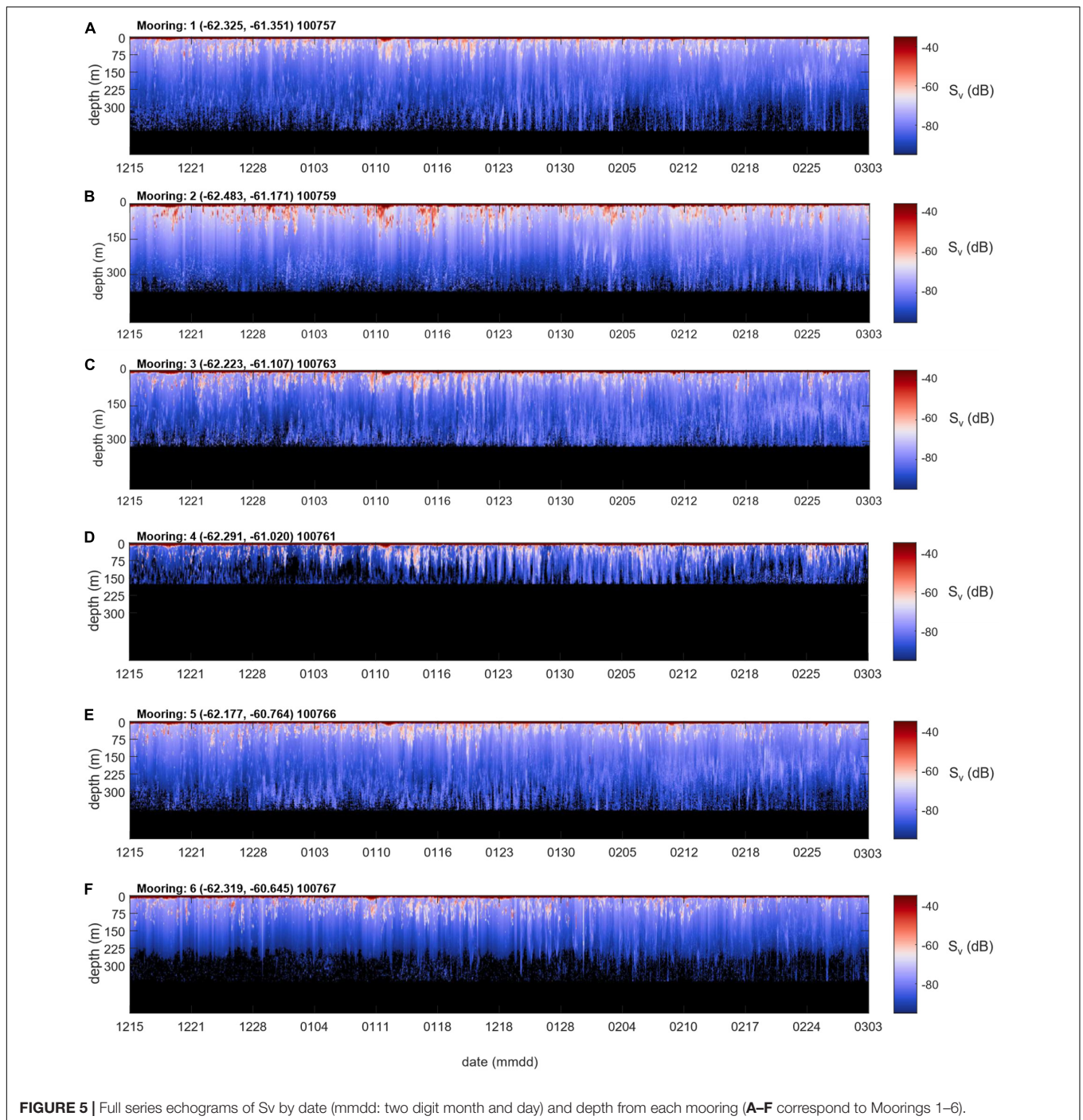
RESULTS

Representative Targets and Patterns in the Echosounder Data

Visual inspection of the echosounder data identified three apparent target types (krill, fish, and indeterminate), all of which exhibited diel vertical migrations but were often separated vertically (e.g., **Figures 3**, **4**). Diel vertical migrations lasted about 1 h and occurred regardless of the sampling month, but, at the latitude of Cape Shirreff where the duration of nighttime ranged from approximately 4 h during December to 8 h by early March, the migrations became more pronounced during the latter half of the study period. Aggregations of target types appeared in layers that were often well separated during daytime. Those with visual characteristics similar to what we consider to be krill swarms were dominant in the upper water column, to a depth of about 150 m. A diffuse and weak scattering layer of unknown

composition occupied the mid depths, typically about 50 m below the maximum depth of krill, and a loose layer of targets that were often individually detected occupied depths from about 200–300 m at the five deep moorings (350 m buoy depth). These same layers were also observed at the shallow mooring (165 m buoy depth), where the different types of targets did occasionally appear to mix during the last month of our study.

Acoustic Data Classification

Target classification based on S_v and dS_v separated the apparent krill, fish, and indeterminate classes (**Figures 3**, **4**). Class-specific values of $< S_v >$ differed by 10–20 dB, and the classification was consistent with our visual interpretation of echograms (**Figure 5**). "Krill" swarms of various morphologies were generally differentiated from other apparent classes of targets (e.g., **Figure 6**), and the S_v data in those regions were retained and used for integrations. However, some regions of the data contained weakly scattering, apparently diffuse targets that may have been sparse, low-density groups of krill occupying areas on the periphery of or outside of denser swarms which may not have been identified as krill by the classifier or were removed by the SNR buffer (e.g., see **Figure 6**).
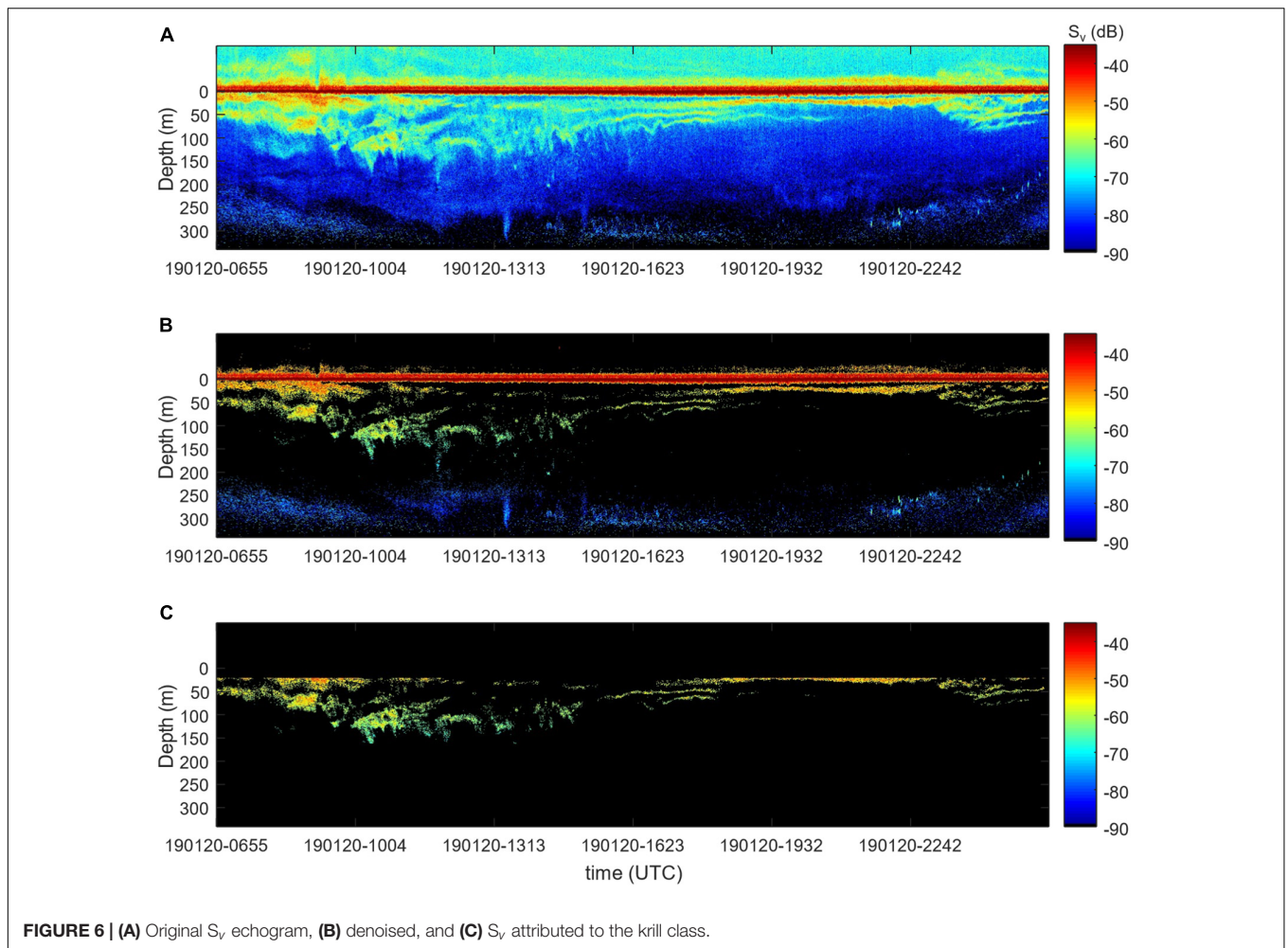
FIGURE 5 | Full series echograms of Sv by date (mmdd: two digit month and day) and depth from each mooring (**A–F** correspond to Moorings 1–6).

S_v Data

Krill swarms are evident in the echograms from all moorings as aggregations of targets with S_v values commonly ranging from approximately −40 to −60 dB and exhibiting daily migrations as deep as about 150 m (**Figure 5**). Krill swarms were observed in various densities at all mooring locations throughout December-March. Although krill are patchy, our data suggest that, off Cape Shirreff, it appears to be more likely to have encountered a patch than not during the 2018/19 austral summer. Nevertheless, S_v varied over the course of our study, and trended downward at all moorings during the study period.

Biomass
Spatial Variation

Among moorings the mean areal biomass density of krill, computed from hourly averages of the narrowband 120 kHz echosounder data, spanned an order of magnitude and ranged from 92 – 399 g·m^{-2} over the study period (**Table 4**), with a grand

FIGURE 6 | (A) Original S$_v$ echogram, **(B)** denoised, and **(C)** S$_v$ attributed to the krill class.

mean over all hourly averages and moorings of 174 g·m^{-2}. The lowest mean biomass was observed at Mooring 1, offshore at the mouth of the western canyon, and the highest mean biomass was observed at Mooring 2, nearshore at the head of the same canyon. Krill swarms observed at Mooring 2 tended to be larger, deeper, and more concentrated than swarms observed at other moorings (**Figure 5**). The same variability between moorings was indicated in time series of daily average biomasses (**Figure 7**) and evident in the overall mean biomass estimates (**Table 4**). The mean biomass at Mooring 6, at the head of the eastern canyon and closer to the predator breeding colonies at Cape Shirreff, was less than half of the biomass at Mooring 2.

Temporal Variation

Biomass densities, $\langle\rho\rangle_{w,a(cw120)}$, measured at 120 kHz and averaged across all six moorings, varied over multiple temporal scales. At time scales of about 5–7 days, daily mean biomass density often increased and then decreased relative to the weekly mean values (**Figure 7**). Only about 6% of the daytime hourly mean biomass values were zero. We also recorded three approximately month-long periods of increasing biomass density followed by relatively strong decreases (**Figure 7**). Despite such

cycling, the daily mean biomass density declined over the entire study period from about 300 g·m^{-2} to 31 g·m^{-2} at a rate of –3.48 g·m^{-2} per day, between mid-December 2018 and early March 2019. Total biomass in the survey area decreased correspondingly, from 211 to 22 kt.

Near-Surface Biomass

Based on data from Moorings 2 and 5, biomass estimates between 10 and 15 m depths represented 13–16% of the total biomass (from 10 to 165 m) during daytime, and 33–35% of the biomass at night (**Table 5**). We excluded nighttime and twilight period data from all our other analyses, but we report the nighttime results here as evidence of diel vertical migration.
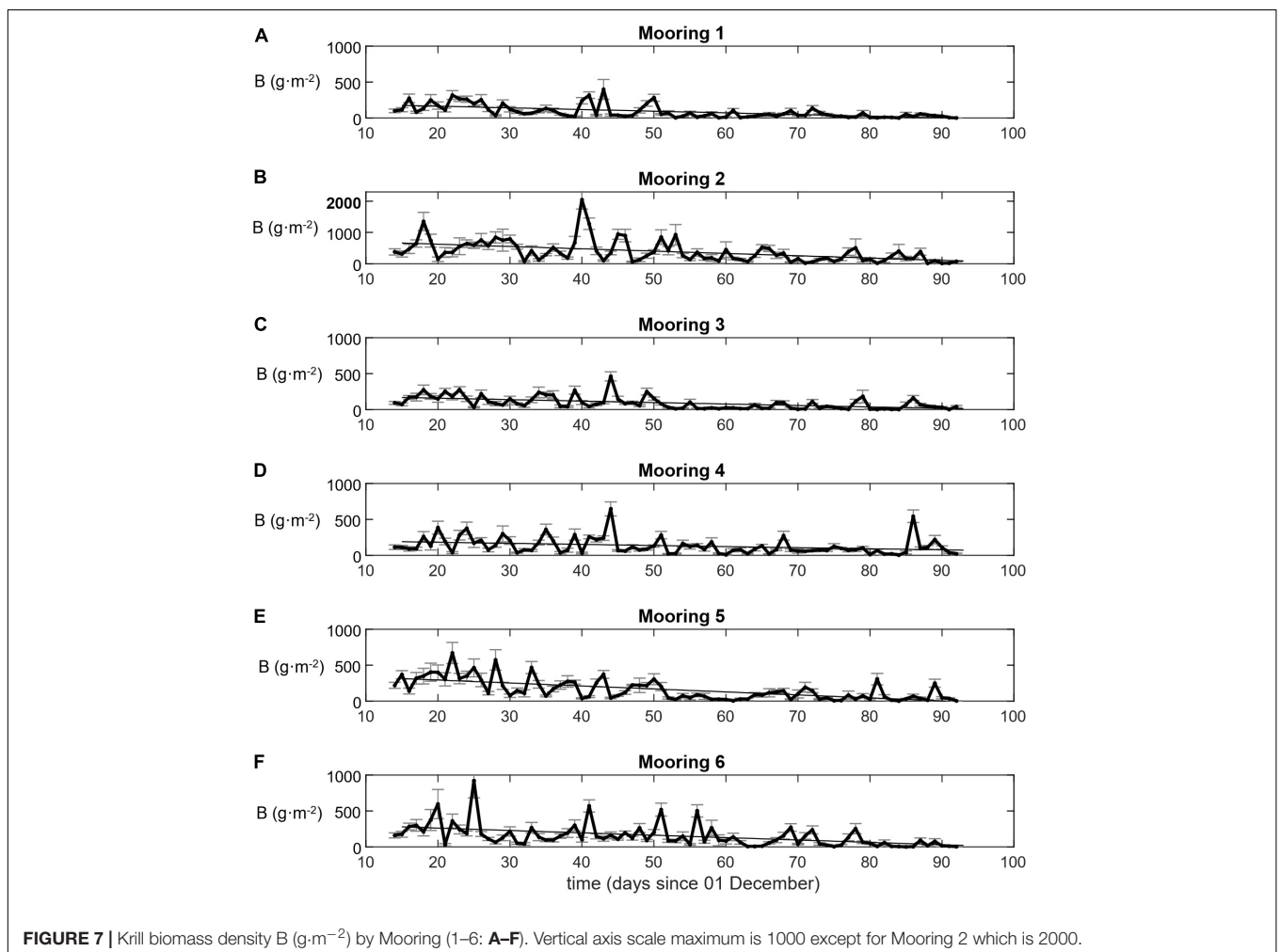
Flow

The time series of velocities among moorings varied over the deployment and contained obvious tidal periodicity (**Table 4** and **Figures 8, 9**). The mean of the flow speed $<|u|>$ from hourly average samples integrated over depths from 40 to 165 m was relatively slow with a grand mean of 0.12 s^{-1}. Daily mean flow increased from 0.10 m·s^{-1} to 0.14 m·s^{-1} over the deployment at a rate of 0.0005 m·s^{-1} per day (**Figure 9**). The highest mean

TABLE 4 | Krill biomass, flux, and flow.

		Mooring						
		1	2	3	4	5	6	Combined
Number of observations		1401	1402	1402	1402	1387	1402	8396
Flow speed (m·s^{-1})	Mean	0.089	0.099	0.133	0.166	0.127	0.103	0.120
	Standard deviation	0.04	0.04	0.05	0.07	0.05	0.03	0.054
	Median	0.08	0.10	0.13	0.16	0.12	0.10	0.108
Flow direction (°)	Mean	−59.4	−52.3	−94.6	−75.9	−92.8	0.5	−62.4
	Standard deviation	107.5	118.0	66.3	95.1	96.1	131.3	109.2
	Median	−106.7	−100.5	−110.7	−112.4	−123.5	−31.2	−109.2
	MAD	60.5	77.3	29.1	45.3	30.7	187.0	53.0
Biomass, areal density (g·m^{-2})	Mean	92.0	398.5	94.6	135.0	164.9	159.2	174.1
	Standard deviation	167.3	676.5	156.8	208.5	284.7	303.1	363.3
	Median	22.9	142.7	30.1	57.8	50.6	48.0	47.3
Flux (g·m^{-2}·s^{-1})	Mean	0.051	0.258	0.079	0.151	0.134	0.110	0.130
	Standard deviation	0.095	0.490	0.143	0.261	0.246	0.215	0.280
	Median	0.012	0.081	0.020	0.055	0.036	0.027	0.032

Mean integrated areal biomass density (g·m^{-2}) and flux (g·m^{-2}·s^{-1}) of krill, and flow speed (m·s^{-1}) and direction (°) MAD is median absolute deviation by mooring and over all moorings combined. Biomasses are from the narrowband 120 kHz data; flow magnitudes and directions are from the ADCP data; and fluxes are from the combined 120 kHz and ADCP data. Estimates are for the full study period and based on hourly averages.

FIGURE 7 | Krill biomass density B (g·m^{-2}) by Mooring (1–6: **A–F**). Vertical axis scale maximum is 1000 except for Mooring 2 which is 2000.

flow speed $<|u|>= 0.17$ m·s^{-1} was found at Mooring 4, located on the continental shelf and between the two canyons off Cape Shirreff. The lowest mean flow speed was about 0.10 m·s^{-1} at Moorings 1, near the mouth of the western canyon, and 2 and 6, at the heads of both canyons. Intermediate mean flow speed was observed at Moorings 3 on the slope and 5 near the mouth of the eastern canyon, where $<|u|>= 0.13$ m·s^{-1}.

The current directions, while principally to the southwest for most moorings most of the time, varied among moorings. The median current direction was –109° (or 251°) for all moorings combined. The median current direction for Moorings 1 through 5 ranged from –124° to –101° (236° to 259°), whereas for Mooring 6 the median direction was –31° (329°). Variations of current direction were small for Moorings 3, 4, and 5 with median absolute deviations (MADs) from 29° to 45°, moderate for Moorings 1 and 2, and large for Mooring 6 at the head of the eastern canyon with a MAD of 187° (**Table 4**). The median current direction at Mooring 6 tended to be slightly westward but the mean was close to 0° and flow could be in any direction during a tidal cycle.
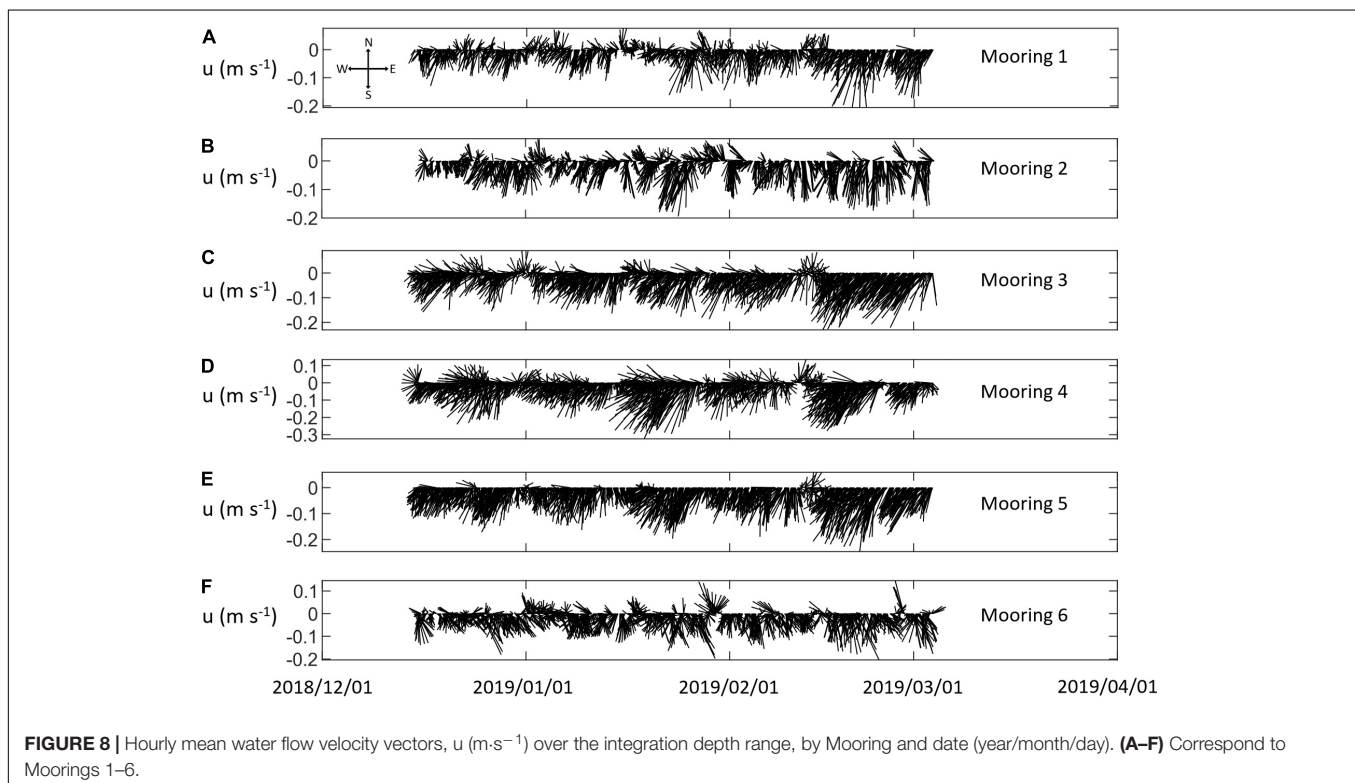
Krill Flux

On a per unit area basis, the mean flux of krill varied by a factor of five among moorings and ranged from 0.05 g·m^{-2}·s^{-1} at Mooring 1 to 0.26 g·m^{-2}·s^{-1} at Mooring 2. The high flux at Mooring 2 was driven by the high biomass there, as the mean flow speed at Mooring 2 was actually less than the overall mean flow speed. The grand mean krill flux over all hourly samples was 0.13 g·m^{-2}·s^{-1} (std. dev. = 0.28 g·m^{-2}·s^{-1},

TABLE 5 | Comparison of biomass in the near-surface (10–15 m) to full (15–165 m) integration depth ranges.

	Mooring 2	Mooring 5
Day only:	(g m^{-2})	(g m^{-2})
Mean(B10-15m, day)	61.43	32.02
Mean(B15-165m, day)	398.54	164.90
Mean(Btotal, day)	459.96	196.92
Night only:		
Mean(B10-15m, night)	51.42	10.88
Mean(B15-165m, night)	106.06	20.57
Mean(Btotal, night)	157.48	31.44
Ratios mean(B10-15m)/mean(Btotal):		
Mean(B10-15m)/mean(Btotal) (day)	0.13	0.16
Mean(B10-15m)/mean(Btotal) (night)	0.33	0.35

median = 0.03 g·m^{-2}·s^{-1}) (**Table 4**). An above average flux (0.15 g·m^{-2}·s^{-1}) was observed on the shelf at Mooring 4, but the flux at Mooring 3, immediately offshore of Mooring 4 and on the slope, was below average (0.08 g·m^{-2}·s^{-1}). Flux at the eastern Moorings 5 and 6 were 0.13 g·m^{-2}·s^{-1} and 0.11 g·m^{-2}·s^{-1} respectively, at or below average for the area. Daily mean krill flux ranged from 0.02 to 0.31 g·m^{-2}·s^{-1} and followed a decreasing trend over the study period (**Figure 9**). This trend was driven by the overall decrease in biomass density because, though variable, flow velocities slowly increased over the study period (**Figure 9**). An ordinary least squares regression fitted to hourly fluxes from all moorings combined estimated that mean daily flux decreased
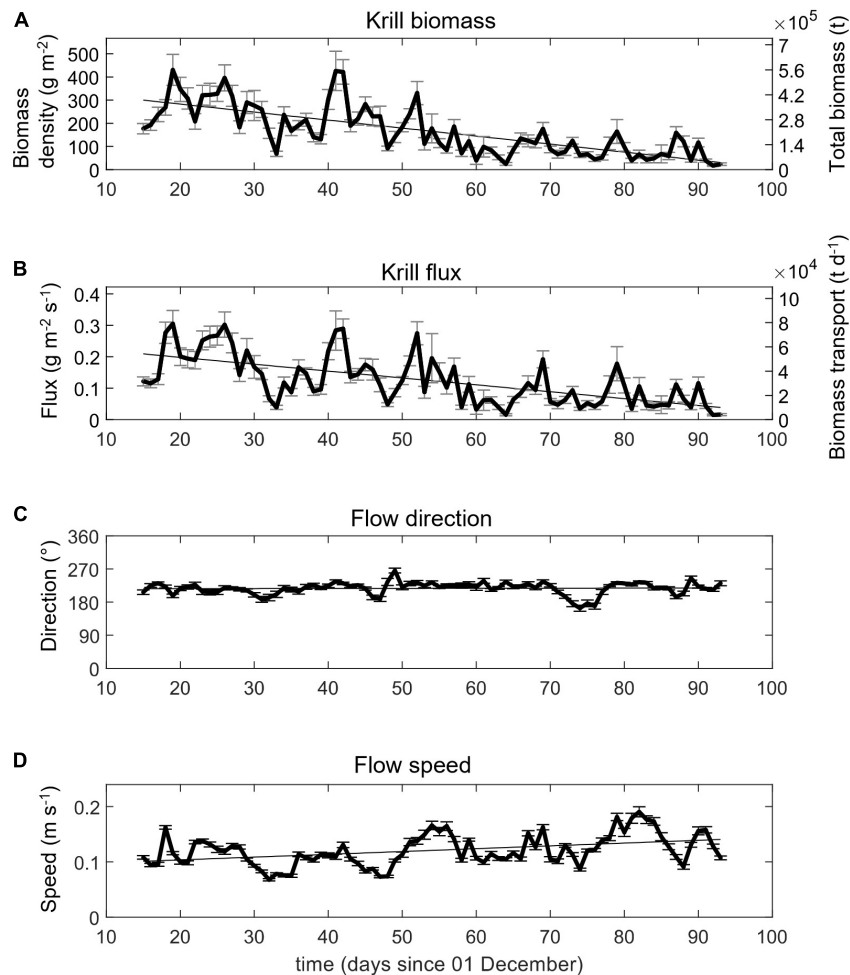

FIGURE 8 | Hourly mean water flow velocity vectors, u (m·s^{-1}) over the integration depth range, by Mooring and date (year/month/day). **(A–F)** Correspond to Moorings 1–6.

FIGURE 9 | Daily mean **(A)** krill biomass density (g m^{-2}) [left axis] and total biomass (t) [right axis], **(B)** krill flux (g m^{-2} s^{-1}) [left axis] and daily mean biomass transport (t d^{-1}), **(C)** flow direction (°), and **(D)** flow speed (m s^{-1}).

from 0.22 g·m^{-2}·s^{-1} on 15 December 2018 to 0.04 g·m^{-2}·s^{-1} on 3 March 2019, at a rate of –0.0023 g·m^{-2}·s^{-1} per day over the study period. Thus, total daily biomass transport decreased from about 54 × 10^3 t·d^{-1} in late December 2018 to about 10 × 10^3 t·d^{-1} by early March 2019. Total daily transport reached at least 70 × 10^3 t·d^{-1} on four occasions, all before the end of January 2019, and fell below 5 × 10^3 t·d^{-1} on 3 days later in the study period. As with biomass density, daily total transport also increased and decreased over periods of about 5–7 days (see **Figure 9**).

Based on the grand mean flux (from hourly averages) of 0.13 g·m^{-2}·s^{-1} and the 20 km by 150 m vertical cross section of our study area, over the entire 79-day survey period (15 December – 3 March) the total cumulative krill biomass passing through the study area was about 2.5 million ton. This estimate of overall cumulative biomass flow through the study area considers all daily averages of biomass and mean flow speed and direction as constants but allows a simple representation of the biomass flow through the region and is justified by the long-period mean flow speed and direction being similar among moorings.

Transport Paths

Eleven weekly progressive vector diagrams (PVDs), generated from combining the velocity data with the hourly biomasses (Emery and Thompson, 2014) integrated over the upper 165 m of the water column, demonstrate the patterns of transport driven by mean flow (mooring-based observations) in the study area (**Figure 10**). Three distinct patterns of movement were observed: (1) mainly westward transport from all six moorings, (2) westward transport from four moorings and onshore transport from two nearshore moorings, and (3) westward transport from four moorings and both onshore and offshore transport from two moorings. Transport and presumed passive movement of krill with the prevailing current was principally directed along-shelf to the southwest, based on PVD-indicated displacements from four of the moorings (1, 3, 4, and 5) most of the time. At the two moorings located closer to shore in canyon heads west and east of Cape Shirreff (2 and 6 respectively), displacements were also mostly toward the west but more variable than the other four moorings, and offshore and onshore transport was clearly observed during several periods. For example, displacements

from Moorings 2 and 6 periodically were toward the south and aligned primarily with the canyon axes. This was most obvious in the PVDs from weeks 1 and 11 and part of week 5. During week 7, we observed apparent onshore transport at Mooring 6 (eastern canyon head) and simultaneous offshore transport at Mooring 2 (western canyon head). PVDs from 5 weeks (2, 4, 6, 8, 11) show that movements from five of the six moorings were aligned along-shelf, toward the southwest. These extensive along-shelf displacements coincided with spring tides evident in the high amplitude fluctuations of water pressure and predicted (Pawlowicz et al., 2002) tidal amplitude (**Figure 10**). Although the PVDs indicate that movement from Mooring 6 was more southward during those same weeks, data from underwater gliders deployed in the area (Reiss et al., 2021) indicated that the current between Mooring 6 and shore was strongly toward the west. Thus, although the PVDs suggest southern displacements from Mooring 6, the actual paths may have deviated westward.

DISCUSSION

We used an array of six subsurface ADCPs with integrated wideband echosounders to measure the biomass and flux of krill during the austral summer of 2018–2019 near an important and long-studied predator colony (e.g., Hinke et al., 2017; Krause et al., 2020; Watters et al., 2020) in the South Shetland Islands, Antarctica. We discriminated apparent krill aggregations from other scatterers using a classifier derived from the wideband echosounder. Our moorings provided detailed information about the temporal variations of biomass and transport of krill in a manner not resolved using conventional, transect-oriented, ship-based surveys. Observed declines in krill biomass density suggest that the prey field available to krill-dependent predators can vary greatly within the austral summer while the spatial variability of mean biomass density suggests potentially differential benefits to predators and profitability to fisheries within relatively small areas on the continental shelf.

Calibrations and Validations

We converted the recorded power amplitude of the Signature100 echosounders to calibrated volume backscattering strength S_v. This allowed us to use standard models to estimate numerical and biomass density of targets like krill based on existing target strength models, but these results all depend on accurate calibration gain offsets. We believe our calibration gain offsets were accurate. In addition to estimating calibration gain offsets in the highly controlled environment of the laboratory tank (Demer et al., 2015b), we compared the echo returns from the water surface, as observed by different moorings during overlapping time periods. While surface conditions may vary on a short-term basis between moorings, the surface of the entire study area was affected similarly by winds over many hours or days, and the characteristics of the S_v distributions of the surface recorded by all moorings should be similar enough to determine if the calibration gain offset of any single mooring was grossly in error. S_v distributions representing surface echoes received among all moorings during the same time periods had similar

mean values and were between −1.0 and +1.1 dB of $<S_v>$ for surface echoes from the narrowband 120 kHz channel. This range is relatively narrow considering that the moorings were separated by distances of tens of kilometers, and all but one were submerged 350 m below the surface. Furthermore, our comparisons of surface S_v include three time periods between mid-December and early February, over which winds and surface conditions varied, and the surface echo S_v differences were not always higher or lower at any particular mooring. Surface echo S_v from Mooring 5 was higher for most channels during two of these three periods, but the biomass density at Mooring 5 was not significantly different from Moorings 4 or 6. That is, the mean S_v of surface echoes varied with surface conditions more than between moorings, and there was no pattern of bias that would be expected to have been correlated with our biomass estimates.

Classification

In addition to the raw acoustic data, the Signature100 recorded data into five wideband frequency bins and two narrowband frequencies that were used to develop models which attempt to discriminate krill from other scatterers. Differences of mean volume scattering strength, dS_v, between two or more frequencies are often used to discriminate acoustic targets of interest in fisheries (Madureira et al., 1993; Kang et al., 2002; Jech et al., 2018). However, given the frequency bands of the Signature100, dS_v was just 2–3 dB compared to a 10 dB dS_v between 120 and 38 kHz for krill of lengths near the mean length we observed. So typical dB-differencing approaches would not be useful. However, given that the predicted, frequency-specific krill TS and S_v varied up to 3 dB for frequency bands of the Signature100 (Amakasu et al., 2017), we used distributions of S_v and dS_v from each frequency band to develop a supervised, minimum distance classifier to discriminate krill from fish or other zooplankton.

Other classification methods for krill have proven successful (Kitamura et al., 2017; Jech et al., 2018; Brautaset et al., 2020), and our method is conceptually similar to using a combination of dS_v and a multi-frequency single-beam index (Jech and Michaels, 2006; Jech et al., 2018) without explicit calculation of a multi-frequency index value (Trenkel and Berger, 2013; Wall et al., 2016). We did not use theoretical models of target strength (as for the DWBA-Z-score method of Jech et al., 2018) as a basis for class-specific feature distributions, as that approach would have required many assumptions that might introduce additional uncertainty or bias because, although it was important to exclude non-krill scatterers, we did not try to identify the other target types.

We had three goals for our classifier. First, we needed to eliminate other major scatterers from being included in our estimates of krill biomass. Second, we wanted to avoid delineating krill swarms based on visual scrutinization. Third, we wanted to automate the process of identifying krill in a manner comparable to that which an expert analyst might do via visual scrutinization. Together, any misclassification errors in our automated approach would apply to the data from all moorings and not affect results from one mooring differently than others. The use of the dS_v in combination with S_v values among frequency bands measured by the Signature100 was sufficient to provide consistent
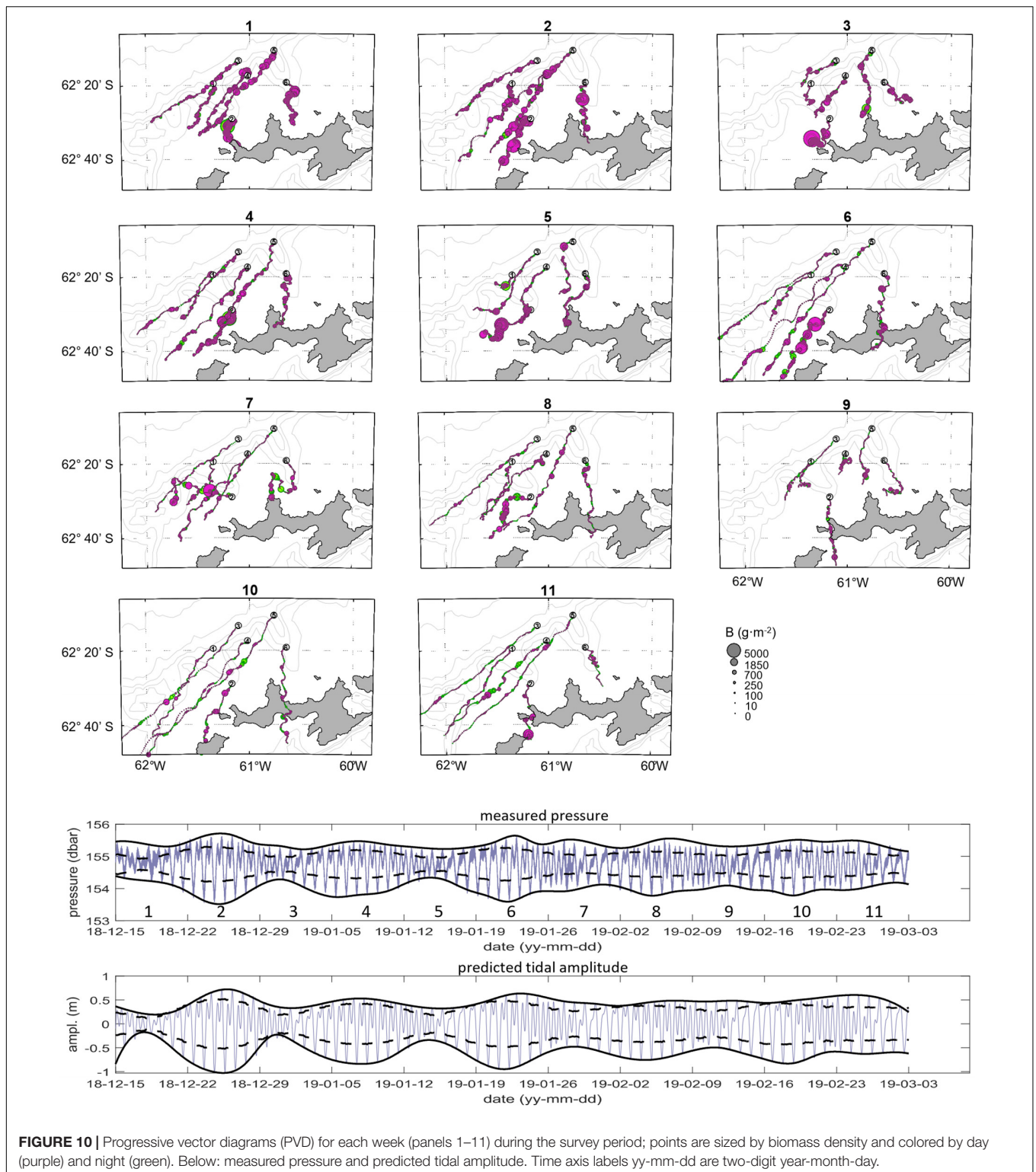
FIGURE 10 | Progressive vector diagrams (PVD) for each week (panels 1–11) during the survey period; points are sized by biomass density and colored by day (purple) and night (green). Below: measured pressure and predicted tidal amplitude. Time axis labels yy-mm-dd are two-digit year-month-day.

classification and discrimination of apparent krill from the other target types in our data (**Figures 4**, **6**). This enabled automatic assignment of data to the krill class and allowed us to make biomass estimates specific to targets we believe are krill.

Visual identification of krill swarms is relatively easy for dense and isolated swarms and also possible for more dispersed, loosely aggregated, or "dynamic and patchy" swarms as described by Fallon et al. (2016). Species-composition data from targeted

trawls suggest that swarms of various morphologies and appearances, such as those we observed, are nearly or totally *Euphausia* spp. and are dominated by *E. superba* (Fallon et al., 2016). Although other smaller and/or weaker scatterers may be present and represented by features in the echograms, we assume that the apparent krill swarms are euphausiids (Fallon et al., 2016).

We compared figures representing unfiltered S_v, "denoised" S_v, and krill-class masked echograms and rarely found target patches that did not appear to be krill. Such features were small relative to the typical spatial-temporal extent of obvious krill swarms and occurred only a small fraction of the time. Their effect on integrated biomass values were negligible. Also, based on experiments comparing classified to unclassified data, using a conservative level of SNR threshold criteria (10 dB), limiting data integration to a maximum depth of 165 m, and excluding night-time data results in relatively small increases of biomass if data are not processed by class and other weak scatterers are not excluded. That is, echoes consistent with krill dominated the scattering in our study area during the day down to about 150 m below the surface, and if range-dependent noise were removed with a large SNR threshold the residual data represented what we consider to be krill swarms.

Ultimately, our classification method is unvalidated beyond visual scrutinization of the classified echograms to ensure consistency with what we have observed in echograms from years of ocean surveys, and from previously described characteristics of aggregations that contained 100% euphausiids based on targeted net tows (Fallon et al., 2016). Comparisons to other approaches (e.g., Coetzee, 2000), now being used in the Antarctic (Krafft et al., 2021) could be useful in the future, if we can accumulate sufficient *in situ* data to definitely identify krill.

Our main goal for classification was to retain krill and eliminate the "fish" echoes, presumably representing fish without swim bladders, from inclusion in biomass estimates, and our classifier appeared to do this consistently but was practically unnecessary for five of our six moorings. Except for shallow mooring 4, submerged at about 165 m depth, most of our echosounder data were adequately parsed into krill-like vs. other sources simply by removing noise and applying a SNR threshold and depth-range limits. Most data remaining within the integration depth range after noise removal and prior to classification represented krill-class targets (**Figure 6**). If future validation data confirm this, then it suggests that swarm-oriented classification methods (Coetzee, 2000) using even single frequency data (Krafft et al., 2021) may be sufficient for estimating Antarctic krill biomass density. However, multiple frequency and wideband data may still be preferable because they allow estimation of other important attributes of swarms such as orientation distributions.

Biomass

The overall mean biomass density of krill, over the range of 15–165 m (an integration depth range that is similar to the depth range of krill observed during ship-based acoustic surveys, e.g., Reiss et al., 2008), in our study area during December 2018 and March 2019 was approximately 174 g·m^{-2}. However,

biomass density exhibited substantial spatial (inter-mooring) and temporal variability including a significant decreasing trend from 300 to 31 g·m^{-2} over the season. Thus, the standing biomass in the area decreased from about 211,000 metric tons in December 2018 to 22,000 tons in March of 2019. Short period fluctuations of biomass also occurred throughout the season. Within any 5- to 10-day period, mean biomass often varied by more than a factor of about 2 (**Figure 9**).

The high variability of biomass density at each mooring is indicative of the patchiness of krill aggregations. Patchiness was also evident from averages of biomass over different temporal periods. For example, using daily averages the grand mean biomass density was 142 g·m^{-2}, but it was 174 g·m^{-2} using hourly averages. This effect is caused by local spikes in biomass values being offset by near zero values and is observed in many acoustic times-series (e.g., Brierley et al., 2006; De Robertis et al., 2018). Surface-related echoes, bubbles, predator dives, and sea-ice were not significant sources of variability in our time series measurements based on visual scrutinization of S_v echograms.

For the krill-class regions of our data, we converted the integrated $< s_v >$, or s_a (MacLennan et al., 2002) to krill biomass based on target strength predictions of the DWBA model parameterized using length-frequency data collected from the diets of krill predators foraging in the area and a standard (Hewitt et al., 2004) length-weight relationship. While krill length-frequency distributions are commonly obtained from targeted net tows or systematic trawls during ship-based surveys, the autonomous nature of moorings equipped with only acoustic instruments demands an alternative approach. Reid and Brierley (2001) showed that the length-frequency distribution of krill in diets of predators at South Georgia was similar to that in net tows when krill were large, concluding that diet samples could be used in place of net samples for attributing acoustic energy to krill. Similar relationships have been described near the Antarctic Peninsula (Miller and Trivelpiece, 2007), and, while our moorings were deployed, krill lengths from predator diets were broadly consistent with those collected by ships that were independently surveying the area (Reiss et al., 2021). Additionally, krill may have grown over the deployment period. Between mid-December and February krill are expected to grow approximately 1–2 mm in length, as most growth has ceased by mid to later summer when they spawn (Reiss et al., 2020). This expectation suggests that krill growth during our study period was negligible relative to the measured changes in biomass. If krill did increase in size during the period, then they would have higher TS and the biomass decrease would actually be greater than we estimated. However, target validation and mass conversion will continue to remain a challenge to estimating biomass accurately. Innovative tools and methods that provide improved observations of animals in their environments, e.g., autonomous vehicles equipped with underwater cameras, may offer solutions that reduce uncertainty in biomass estimates.

Comparison of Biomass Estimates From Moorings to Those From Ships and Gliders

Our biomass estimates may seem high relative to results from ship-based surveys conducted in previous years

(Reiss et al., 2008). The average biomass density from 22 surveys of the stratum that includes the shelf where our moorings were deployed was 51 g·m^{-2} and ranged from 0.4 to 141.9 g·m^{-2}. As noted previously, the mean biomass density estimated from our mooring data (174 g·m^{-2}) was more than three times higher than the historical mean from the ship surveys. However, the area surveyed by the ships was substantially larger (~38,500 km^2) than that sampled by our moorings (1,300 km^2). The ship surveys extended from the continental shelf to the open ocean, and most acoustic data recorded by the ships was from offshore areas with low krill densities. Thus, when averaged over the survey area, the mean density is much lower than the biomass density on the shelf where our moorings were located. Nevertheless, our mooring-based biomass estimates are similar to those from a glider-based acoustic survey that overlapped in time and space with our mooring deployment (Reiss et al., 2021). In fact, when the glider data were spatially (within a distance of 0.10 degrees latitude and longitude to any mooring) and temporally matched (within a day) with the mooring data the biomass densities derived from these two platforms were significantly correlated ($p < 0.005$), with mean densities that were within 13% of each other. Finally, we note that, off the northwestern coast of the South Shetland Islands, catches per unit fishing effort achieved by the krill fishery are highest just east and west of our mooring array (Choi et al., 2020). All these data suggest that the high biomass density observed during our study is not uncommon in this area.

Near-Surface Biomass Estimates

Mean biomass density in zone from 10 to 15 m represented 13–16% of the total biomass from 10 to 165 m, during the daytime (based on data from Moorings 2 and 5). These biomass proportions are biased high because we did not attempt to exclude surface related echoes in the 10–15 m depth zone, but these proportions serve as approximate limits of the amount of biomass that might be missed in the near surface during daytime without overwhelming amounts of contamination that occurs closer than 10 m depth. Generally, variation in the biomass estimated from the 10–15 m depth zone followed the pattern of hourly biomass estimated from the 15 to 165 m integration depth range.

During nighttime, biomass density in the 10–15 m depth zone represented about 34% of the total biomass observed from 10 to 165 m. However, the total nighttime biomass in the 10–165 m range was only 16–34% of the daytime total at Moorings 2 and 5. Therefore, approximately 66–84% of the biomass appears to be in the 0–10 m depth range at night.

Inverted moorings might be useful tools for investigating biomass in near-surface zones that might be missed by vessels surveying with hull-mounted echosounders. However, inverted moorings would need to be deployed closer to the surface to better resolve the animals and separate surface effects (e.g., from waves and bubbles), without being so close that the beam might be too narrow to resolve horizontal patchiness. In Antarctica and other areas, shallow moorings are at risk from icebergs, which is one reason our moorings were deployed deep.

Flow

The flow data used for our flux calculations represent the net flow that we measured for the depth range used to integrate S_v data and estimate biomass. Depth profiles of the mean flow speed show that for five of the six moorings, net flow was consistently and clearly to the west ($<u> < 0$) and south ($<v> < 0$) for the entire depth range over which we integrated and where flow was reliably measured (40–165 m) (**Supplementary Figure 1**). For most moorings the depth profiles of $<u>$ and $<v>$ were clearly to the west and south down to depths of at least 300 m. At Mooring 6, the depth profiles show that net flow was generally southward based on $<u>$ being near zero for most of the depth range, however, median u was –31° (**Table 4**) suggesting that net flow there was also westward.

Flux

We estimated krill flux, integrated over 15–165 m, at each mooring and cumulative flux for the study area using the krill biomasses estimated from the combined echosounder and ADCP data provided by our Signature100s. Our estimates of flux are based on an advective transport model characterizing net biomass transport assuming that the effects of active krill movement (e.g., Richerson et al., 2015) are negligible relative to the prevalent flow field when considered over the integration depth range and time periods of our analyses. Flux was predominantly toward the southwest direction (along the continental shelf), with a mean flow that averaged about 0.1 m·s^{-1} during December and increased by 20% over the season (**Figure 10**). Mean net flux of krill was 0.13 g·m^{-2}·s^{-1}, which converts to a biomass transport of 32,120 tonne·d^{-1} through the entire study area. Flux varied among moorings and followed a decreasing trend, like the biomass, opposite to the increasing trend in flow speed. Although local residence times and fluxes may be complicated by the combination of vertical migrations and variable, tidally influenced flow velocity over depth and time, the consistency of the flow vectors over time (**Figure 8**) suggest that our simplified model may adequately represent the system for characterizing net flux.

The depth profiles of flow at Mooring 6 suggest that transport could be toward the south, toward the eastern side of Cape Shirreff. However, gliders deployed during this study in the area (Reiss et al., 2021) encountered a strong westward flowing current between Mooring 6 and the shore at Cape Shirreff to the south. Hence the flow at mooring 6 might be influenced by its location in the head of the canyon, but nearby shelf flows still appear to be net westward but are tidally influenced and constrained by the island and nearshore bathymetry. Therefore, the flow patterns near Mooring 6 may induce extended residence times for krill near Cape Shirreff during some tidal periods but then reduce residence times during others. We plan to examine this in further detail by analyzing individual mooring data and data from future deployments.

Mean water flow direction and krill flux along the shelf off Cape Shirreff during the austral summer is westward and in the opposite direction of the offshore currents (Antarctic Circumpolar Current) and presumed transport pathways of krill (Hoffman and Murphy, 2004) originating from the

Bellingshausen Sea. This finding is similar to results from circulation modeling studies (Piñones et al., 2011; Jiang et al., 2013). There was no evidence of large on-shelf net displacements of water and krill in our data (**Figure 9**), suggesting the krill in our study area were not directly supplied from a large population in the Bellingshausen Sea.

Mean daily flux decreased from approximately 0.3 g·m^{-2}·s^{-1} to 0.05 g·m^{-2}·s^{-1} between December and March, but flux also varied over shorter time scales (**Figure 9**). The cyclic, tidally driven flow patterns that we observed may influence short-term trajectories of krill swarms. Most of the short-period fluctuations of flux followed those of biomass, but there were several instances where changes in flow magnitude clearly altered the pattern, with higher and lower flow rates leading to relatively higher and lower fluxes, respectively.

Total Mass Transport, in Context

Although our estimate of cumulative mass transport through the study area (2.5 million ton of krill over the entire sampling period) may seem high, complementary calculations using ship- or glider-based biomass density estimates restricted to the shelf and assuming a constant flow speed of 0.1 m·s^{-1} produce comparable results. Our estimate of cumulative mass transport is also consistent with earlier ship-based research conducted in Bransfield Strait (Everson and Murphy, 1987). We believe our results are plausible, but it is important not to confuse integrated biomass flux with standing stock biomass. Our estimates of biomass and flux do not indicate that the krill resource is more plentiful than previously thought, nor that krill availability should be considered inexhaustible. Our results simply indicate that large quantities of krill may move along the shelf region near the South Shetland Islands. Our cumulative estimate of 2.5 million tons of krill biomass transported through this area, based on mooring data, represents approximately 20–40% of the long-term mean standing stock biomass of krill occurring around the South Shetland Islands during the austral summer (Reiss et al., 2008; Macaulay et al., 2020).

Our approach to estimate flux resembles that of Murphy et al. (2004), except their data were collected from a mobile platform (a ship) transiting a 160-km transect and they used CTD data in combination with ADCP data to estimate the total velocity field from the sum of the calculated geostrophic and ageostrophic components. Their results suggest that the total krill flux along the transect was 106 g s^{-1} during their sampling period, or 154 to 200×10^3 t·d^{-1}. We estimated krill flux to be 45×10^3 t·d^{-1} across a 20-km wide and 150-m deep cross-shelf section. The net flux estimates of Murphy et al. (2004) were strongly influenced by a dense swarm of krill with densities on the order of 10 g·m^{-3} found at 60–80 m depth in a location where the flow rate was approximately 0.3–0.35 m·s^{-1} (their **Figure 3**). Our near instantaneous, sample-based estimates of krill biomass density indicate short periods (seconds to minutes) when the maximum value of integrated krill densities were as high as approximately 20×10^3 g·m^{-2}, or a volumetric average density of about 130 g·m^{-3} over our 150-m integration range. Our maximum hourly average krill biomass was about 4×10^3 g·m^{-2} (**Figure 7**) or about 25 g·m^{-3}.

Transport and Apparent Connectivity

Pulses of high biomass appeared at different moorings lagged in time by about the same period that the mean flow speed and direction indicated that advective transport would occur between moorings. The predicted displacement trajectories from the PVD results also suggested that large swarms with high biomass observed at "upstream" moorings are subsequently observable at "downstream" moorings about 2–4 days later. This was evident most often between Moorings 5, at the northeast corner of our array, and 4, in the center, which were the two moorings most closely aligned with the mean flow direction. We do not think we observed the same groups of individual krill at downstream locations but that krill swarms which cover areas of a few square km are sometimes large enough and maintain average densities over time periods of days. These observations seem to confirm consistency with mostly passive transport of swarms between moorings, during summer. Without the flow data from the ADCP, these corresponding pulses of biomass among moorings would be difficult to identify because of the complexities of flow paths. In some cases when a large biomass pulse did not recur at a downstream mooring the PVD suggested that flow deviated away from the downstream location. In other cases when we did not observe biomass pulses at downstream moorings the PVDs may have included error (Tapia et al., 2004; Carlson et al., 2010) or the PVDs may have indicated correct flows but active movements of krill (e.g., Richerson et al., 2015) led to dispersal or reorganization of swarms between moorings.

Our mooring data document swarms spanning many hours, with densities from 1 to about 20 kg·m^{-2} (instantaneous). The duration of some observations (up to 16h) combined with the mean flow speed of about 0.1–0.14 m·s^{-1} suggests that the swarms we observe, although usually small (about 100 m extent in the horizontal) can span distances on the order of 3–5 km in the along-current direction. If we consider swarms to horizontally isometric, then it is plausible that some of the same large swarms can be observed 18 km away, at another mooring after about 2–3 days and with similar temporal density patterns. That is, even if the trajectory is not exactly from mooring to mooring, some part of these large swarms could be observable "downstream" at a later time. Of course, it seems likely that such large aggregations often break up and recombine (coalesce), perhaps on a daily basis. In this case, large swarms would still be expected to be observed downstream, but perhaps with gaps between apparently smaller aggregations. The opposite could be happening as well, i.e., multiple swarms combining into a single large swarm. Regardless, the large pulses that we observed in the time series of biomass spanned periods of time sufficient to indicate krill aggregations that sometimes covered about 10–25 km^2 and were detectable at a downstream location within a few days.

Importance for Predators

Large decreases in biomass like we observed may require that krill-dependent predators increase foraging effort and energy expenditures or seek alternative prey in response to diminishing krill resources. Such shifts in predation strategies may occur during critical periods within predator life cycles (e.g., Hinke et al., 2017) and potentially have negative effects on predator

performance (e.g., Watters et al., 2020). We measured large differences in mean biomass at the heads of the western and eastern canyons (Moorings 2 and 6, respectively). On average, there was about 3–4 times more biomass at Mooring 2 than the other moorings, suggesting that different dynamics influenced biomass transport and accumulation at the two canyon heads. This might affect krill availability to predators or the fishery.

The degrees to which changes in flux benefit or stress predators is unclear. For instance, increased flux may benefit predators by providing more krill prey within shorter periods and apparently be beneficial, yet the increased flow speed may require more energy expenditure if the predators are swimming against the current. Alternatively, decreased flux might make less krill biomass available to predators, but we do not know what level of decrease might affect the predators. Predator-prey relationships have previously been studied in the context of seasonally- and spatially-integrated estimates of krill biomass, usually developed from "synoptic" ship-based surveys designed to advise management of the krill fishery. These surveys, coupled with detailed information about predator foraging (e.g., Hinke et al., 2017), have had mixed results (e.g., Watters et al., 2020) in part because the ship surveys do not cover nearshore areas with the highest foraging rates (consider Figure 6 of Hinke et al., 2017). Our moorings now enable us to better document the spatio-temporal distribution of krill patches and their flux at an increased, more "predator-relevant," resolution. The prey field can now be observed with similar detail as the dynamics of predator foraging. Using data from these moorings and future deployments of animal-borne instruments that can be used to characterize foraging dynamics, we will examine foraging near moorings to better describe relationships between predator behaviors and krill swarms.

Additionally, gliders (Reiss et al., 2021) or other autonomous data collection methods (Harcourt et al., 2019) can be used to measure hydrographic properties in the water column above the sub-surface moorings, providing other critical data (primary production and water column temperature) that can influence prey behaviors. Together, instruments like these ADCP echosounder mooring systems can supply data needed for to inform integrated ecosystem monitoring programs (e.g., Brautaset et al., 2020).

CONCLUSION

We have demonstrated the use of integrated wideband echosounder and ADCP instruments (Nortek Signature100) to simultaneously measure currents, estimate krill biomass, and the krill flux in an area that is important to foraging predators and a commercial fishery. Trends of mean daily biomass and flux both decreased significantly from December 2018 to March 2019, and flux decreased despite an increase of mean daily current

magnitude. Such long-term, fine-scale data can be useful for developing ecosystem approaches to fisheries management when there is a need to quantify the relative importance of fishing and environmentally driven changes in prey availability on predator performance over multiple time and space scales. In the Antarctic, fishing can have plausible effects on predators at scales smaller than those that are currently used for establishing catch limits (Plagányi and Butterworth, 2012; Krüger et al., 2020; Watters et al., 2020), and managers are concerned with the potential for fishing to result in locally high exploitation rates. Therefore, high-resolution measurements collected by moorings like those used here, deployed in critical fishing areas, can provide data to better understand ecosystem dynamics without committing vessel time to continuous or repeated surveys.

DATA AVAILABILITY STATEMENT

The raw data supporting the conclusions of this article will be made available by the authors, without undue reservation.

AUTHOR CONTRIBUTIONS

GW, CR, and GC designed the study. GC and CR designed and deployed the moorings and drafted the manuscript. GC programmed the ADCP instruments and analyzed the mooring data. SN provided technical information about the echosounders' onboard data processing, enabled raw data collection, and reviewed calibration code. All authors contributed to revisions leading to the submitted version.

ACKNOWLEDGMENTS

SUPPLEMENTARY MATERIAL

The Supplementary Material for this article can be found online at: https://www.frontiersin.org/articles/10.3389/fmars.2022.784469/full#supplementary-material

Supplementary Figure 1 | Depth profiles of mean S_v, u, and v for each mooring, with horizontal lines marking the depth limits of S_v integration (15 and 165 m) and flow speed averaging (40 and 165 m) and vertical lines marking $S_v = -75$ dB and u, $v = 0$ m s^{-1}.

REFERENCES

Amakasu, K., Mukai, T., and Moteki, M. (2017). Measurement of the volume-backscattering spectrum from an aggregation of Antarctic krill and inference of their length-frequency distribution. *Polar Sci.* 12, 79–87. doi: 10.1016/j.polar.2017.02.007

Atkins, P., Francis, D., and Foote, K. (2008). Calibration of broadband sonar systems using multiple standard targets. *J. Acoust. Soc. Am.* 123:3436. doi: 10.1121/1.2934223

Bestley, S., Ropert-Coudert, Y., Nash, S., Brooks, C., Cotte, C., Dewar, M., et al. (2020). Marine ecosystem assessment for the southern ocean: birds and marine mammals in a changing climate. *Front. Ecol. Evolu.* 8:566936. doi: 10.3389/fevo.2020.566936

Brautaset, O., Waldeland, A. U., Johnsen, E., Malde, K., Eikvil, L., Salberg, A., et al. (2020). Acoustic classification in multifrequency echosounder data using deep convolutional neural networks. *ICES J. Mar. Sci.* 77, 1391–1400. doi: 10.1093/icesjms/fsz235

Brierley, A. S., Saunders, R. A., Bone, D. G., Murphy, E. J., Enderlein, P., Conti, S. G., et al. (2006). Use of moored acoustic instruments to measure short-term variability in abundance of Antarctic krill, Limnol. *Oceanogr. Methods* 4:18. doi: 10.4319/lom.2006.4.18

Carlson, D. F., Muscarella, P. A., Gildor, H., Lipphardt, B. L., and Fredj, E. (2010). How useful are progressive vector diagrams for studying coastal ocean transport, Limnol. *Oceanogr. Methods* 8:98. doi: 10.4319/lom.2010.8.0098

Choi, S.-G., Chae, J., Chung, S., Oh, W., Yoon, E., Sung, G., et al. (2020). Density estimation of antarctic krill in the south shetland island (subarea 48.1) using db-difference method. *Sustainability* 12:5701. doi: 10.3390/su12145701

Clay, C. S., and Medwin, H. (1977). *Acoustical Oceanography: Principles and Applications.* New York: Wiley, 544.

Cochrane, N. A., Li, Y., and Melvin, G. D. (2003). Quantification of a multibeam sonar for fisheries assessment applications. *J. Acoust. Soc. Am.* 114, 745–758. doi: 10.1121/1.1587151

Coetzee, J. (2000). Use of a shoal analysis and patch estimation system (SHAPES) to characterize sardine schools. *Aquatic Living Res.* 13, 1–10.

Cutter, G. R., Renfree, J. S., Cox, M. J., Brierley, A. S., and Demer, D. A. (2009). Modelling three-dimensional directivity of sound scattering by Antarctic krill: progress towards biomass estimation using multibeam sonar. *ICES J. Mar. Sci.* 66, 1245–1251.

De Robertis, A., and Higgenbottom, I. (2007). A post-processing technique to estimate the signal-to-noise ratio and remove echosounder background noise. *ICES J. Mar. Sci.* 64, 1282–1291.

De Robertis, A., Levine, R., and Wilson, C. D. (2018). Can a bottom-moored echo sounder array provide a survey-comparable index of abundance? *Can. J. Fish. Aquat. Sci.* 75, 629–640. doi: 10.1139/cjfas-2017-0013

De Robertis, A., McKelvey, D. R., and Ressler, P. H. (2010). Development and application of an empirical multifrequency method for backscatter classification. *Can. J. Fish. Aquat. Sci.* 67, 1459–1474. doi: 10.1139/F10-075

Demer, D. A., Berger, L., Bernasconi, M., Bethke, E., Boswell, K., Chu, D., et al. (2015a). Calibration of acoustic instruments. *ICES Cooperat. Res. Rep. No. 326:133.*

Demer, D. A., Cutter, G. R. Jr., Stierhoff, K. L., and Renfree, J. S. (2015b). Two-million-liter tank expands the boundaries of marine technology innovation: national resource available for advancing marine science. *Mar. Technol. Soc. J.* 49:9. doi: 10.4031/MTSJ.49.2.9

Emery, W., and Thomson, R. (2014). *Data Analysis Methods in Physical Oceanography,* 3rd Edn. Waltham, MA: Elsevier.

Everson, I., and Murphy, E. (1987). Mesoscale variability in the distribution of krill euphausia superba. *Mar. Ecol. Prog. Ser.* 40, 53–60. doi: 10.3354/meps040053

Fallon, N. G., Fielding, S., and Fernandes, P. G. (2016). Classification of Southern ocean krill and icefish echoes using random forests. *ICES J. Mar. Sci.* 73, 1998–2008. doi: 10.1093/icesjms/fsw057

Fielding, S., Watkins, J., Trathan, P. N., Enderlein, P., Waluda, C. M., Stowasser, G., et al. (2014). Interannual variability in Antarctic krill (*Euphausia superba*) density at south georgia, southern ocean: 1997–2013. *ICES J. Mar. Sci.* 9, 2578–2588. doi: 10.1093/icesjms/fsu104

Foote, K. G., Knudsen, H. P., Vestnes, G., MacLennan, D. N., and Simmonds, E. J. (1987). *Calibration of Acoustic Instruments for fish Density Estimation: A Practical Guide ICES, Cooperative Research Report No. 144.*

Godø, O., Reiss, C. S., Siegel, V., and Watkins, J. (2014). Commercial fishing vessel as research vessels in the antarctic – requirements and solutions exemplified with a new vessel. *CCAMLR Sci.* 21, 1–12.

Greene, C. H., Meyer-Gutbrod, E. L., McGarry, L. P., Hufnagle, L. C., Chu, D., McClatchie, S., et al. (2014). A wave glider approach to fisheries acoustics: transforming how we monitor the nation's commercial fisheries in the 21st century. *Oceanography* 27, 168–174. doi: 10.5670/oceanog.2014.82

Handegard, N. O., Buisson, L. D., Brehmer, P., Chalmers, S. J., De Robertis, A., Huse, G., et al. (2012). Towards an acoustic-based coupled observation and modelling system for monitoring and predicting ecosystem dynamics of the open ocean. *Fish Fish* 14, 605–615. doi: 10.1111/j.1467-2979.2012.00480.x

Harcourt, R., Sequeira, A. M. M., Zhang, X., Roquet, F., Komatsu, K., Heupel, M., et al. (2019). Animal-borne telemetry: an integral component of the ocean observing toolkit. *Front. Mar. Sci.* 6:326. doi: 10.3389/fmars.2019.00326

Hewitt, R., Demer, D., and Emery, J. (2003). An 8-year cycle in krill biomass density inferred from acoustic surveys conducted in the vicinity of the south shetland Islands during the austral summers of 1991–1992 through 2001–2002. *Aquat. Living Res.* 16, 205–213. doi: 10.1016/S0990-7440(03)00019-6

Hewitt, R. P., Watkins, J., Naganobu, M., Sushin, V., Brierley, A. S., Demer, D., et al. (2004). Biomass of antarctic krill in the scotia sea in january/february 2000 and its use in revising an estimate of precautionary yield. *Deep Sea Res. Part II Top. Stud. Oceanogr.* 51, 1215–1236.

Hinke, J. T., Cossio, A. M., Goebel, M. E., Reiss, C. S., Trivelpiece, W. Z., and Watters, G. M. (2017). Identifying risk: concurrent overlap of the antarctic krill fishery with krill-dependent predators in the scotia sea. *PLoS One* 12:e0170132. doi: 10.1371/journal.pone.0170132

Hoffman, E. E., and Murphy, E. J. (2004). Advection, krill, and antarctic marine ecosystems. *Antarct. Sci.* 16, 487–499. doi: 10.1017/s0954102004002275

Jech, J., Horne, J., Chu, D., Demer, D., Francis, D., Gorska, N., et al. (2015). Comparisons among ten models of acoustic backscattering used in aquatic ecosystem research. *J. Acoust. Soc. Am.* 138, 3742–3764. doi: 10.1121/1.4937607

Jech, J. M. (2011). Interpretation of multi-frequency acoustic data: effects of fish orientation. *J. Acoust. Soc. Am.* 129, 54–63. doi: 10.1121/1.3514382

Jech, J. M., Gareth, L. L., and Andone, C. L. (2017). Wideband (15–260 kHz) acoustic volume backscattering spectra of northern krill (*Meganyctiphanes norvegica*) and butterfish (*Peprilus triacanthus*). *ICES J. Mar. Sci.* 74, 2249–2261. doi: 10.1093/icesjms/fsx050

Jech, J. M., Lawson, G. L., and Lowe, M. R. (2018). Comparing acoustic classification methods to estimate krill biomass in the georges bank region from 1999 to 2012. *Limnol. Oceanogr.: Methods* 16, 680–695.

Jech, J. M., and Michaels, W. L. (2006). A multifrequency method to classify and evaluate fisheries acoustics data. *Can. J. Fish. Aquat. Sci.* 63, 2225–2235. doi: 10.1139/F06-126

Jiang, M., Charette, M. A., Measures, C. I., Zhu, Y., and Zhou, M. (2013). Seasonal cycle of circulation in the antarctic peninsula and the off-shelf transport of shelf waters into southern drake passage and scotia sea. *Deep Sea Res. II* 90, 15–30.

Kang, M., Furusawa, M., and Miyashita, K. (2002). Effective and accurate use of difference in mean volume backscattering strength to identify fish and plankton. *ICES J. Mar. Sci.* 59, 794–804. doi: 10.1006/jmsc.2002.1229

Kinsler, L. E., Frey, A. R., Coppens, A. B., and Sanders, J. V. (1999). *Fundamentals of Acoustics, 4th Edition.* ISBN 0-471-84789-5.

Kitamura, M., Amakasu, K., Kikuchi, T., and Nishino, S. (2017). Seasonal dynamics of zooplankton in the southern chukchi sea revealed from acoustic backscattering strength. *Continental Shelf Res.* 133, 47–58.

Kock, K.-H., Barrera-Oro, E., Belchier, M., Collins, M. A., Duhamel, G., Hanchet, S., et al. (2012). The role of fish as predators of krill (*Euphausia superba*) and other pelagic resources in the southern ocean. *CCAMLR Sci.* 19, 115–169.

Krafft, B. A., Macaulay, G. J., Skaret, G., Knutsen, T., Bergstad, O. A., Lowther, A., et al. (2021). Standing stock of antarctic krill (*Euphausia superba* dana, 1850) (*Euphausiacea*) in the southwest atlantic sector of the southern ocean, 2018–19. *J. Crustac. Biol.* 41:3. doi: 10.1093/jcbiol/ruab046

Krause, D. J., Goebel, M. E., and Kurle, C. M. (2020). Leopard seal diets in a rapidly warming polar region vary by year, season, sex, and body size. *BMC Ecol.* 20:32. doi: 10.1186/s12898-020-00300-y

Krüger, L., Huerta, M. F., Santa Cruz, F., and Cardenas, C. A. (2020). Antarctic krill fishery effects over penguin populations under adverse climate conditions: implications for the management of fishing practices. *Ambio* 50, 560–571. doi: 10.1007/s13280-020-01386-w

Laws, R. M. (1977). Seals and whales of the southern ocean. *Philos. Trans. R. Soc. London Ser. B.* 279, 81–96. doi: 10.1098/rstb.1977.0073

Lawson, G. L., Wiebe, P. H., Ashjian, C. J., Chu, D., and Stanton, T. K. (2006a). Improved parameterization of Antarctic krill target strength models. *J. Acoustic Soc. Am.* 119, 232–242. doi: 10.1121/1.2141229

Lawson, G. L., Wiebe, P. H., Stanton, T. K., and Ashjian, C. J. (2008). Euphausiid distribution along the Western Antarctic Peninsula—Part A: Development of robust multi-frequency acoustic techniques to identify euphausiid aggregations and quantify euphausiid size, abundance, and biomass. *Deep Sea Res. II* 55, 412–431. doi: 10.1121/1.2141229

Lawson, G. L., Wiebe, P. H., Ashjian, C. J., Gallager, S. M., Davis, C. S., and Warren, J. D. (2006b). Acoustically-inferred zooplankton distribution in relation to hydrography west of the antarctic peninsula. *Deep Sea Res II* 51, 2041–2072.

Lee, K., Mukai, T., Kang, D., and Iida, K. (2004). Application of acoustic doppler current profiler combined with a scientific echo sounder for krill euphausia pacifica density estimation. *Fish. Sci.* 70, 1051–1060.

Lunde, P., and Korneliussen, R. J. (2016). Power-budget equations and calibration factors for fish abundance estimation using scientific echo sounder and sonar systems. *J. Mar. Sci. Eng.* 4:43.

Macaulay, G., Skaret, G., Knutsen, T., Bergstad, O. A., Krafft, B., Fielding, S., et al. (2020). Biomass results from the international synoptic krill survey in area 48, 2019. *Rev* 1:2019.

MacLennan, D. N., Fernandes, P. G., Dalen, J., et al. (2002). A consistent approach to definitions and symbols in fisheries acoustics. *ICES J. Mar. Sci.* 59, 365–369. doi: 10.1006/jmsc.2001.1158

Madureira, L. S. P., Ward, P., and Atkinson, A. (1993). Differences in backscattering strength determined at 120 and 38 kHz for three species of antarctic macroplankton. *Mar. Ecol. Prog. Ser.* 93, 17–24. doi: 10.3354/meps093017

Martin-Traykovski, L. V., O'Driscoll, R. L., and McGehee, D. E. (1998). Effect of orientation on the broadband acoustic scattering of antarctic krill (*Euphausia superba*): implications for inverting zooplankton spectral acoustic signatures for angle of orientation. *J. Acoust. Soc. Am.* 104, 2121–2135. doi: 10.1121/1.423726

Meinig, C., Burger, E. F., Cohen, N., Cokelet, E. D., Cronin, M. F., Cross, J. N., et al. (2019). Public private partnerships to advance regional ocean observing capabilities: a saildrone and NOAA-PMEL case study and future considerations to expand to global scale observing. *Front. Mar. Sci.* 6:448.

Miller, A. K., and Trivelpiece, W. Z. (2007). Cycles of *Euphausia superba* recruitment evident in the diet of pygoscelid penguins and net trawls in the south shetland islands, antarctica. *Polar Biol.* 30, 1615–1623. doi: 10.1007/s00300-007-0326-7

Mordy, C. W., Cokelet, E. D., DeRobertis, A., Jenkins, R., Kuhn, C. E., Lawrence-Slavas, N., et al. (2017). Advances in ecosystem research: Saildrone surveys of oceanography, fish, and marine mammals in the bering sea. *Oceanography* 30, 113–115. doi: 10.5670/oceanog.2017.230

Murphy, E. J., Watkins, J. L., Meredith, M. P., Ward, P., Trathan, P. N., and Thorpe, S. E. (2004). Southern antarctic circumpolar current front to the northeast of south georgia: horizontal advection of krill and its role in the ecosystem. *J. Geophys. Res.* 109, 1–10.

Nortek (2021). *Principles of Operation – Signature", 2021, Version 2021.1.*

Pawlowicz, R., Beardsley, B., and Lentz, S. (2002). Classical tidal harmonic analysis including error estimates in MATLAB using T_TIDE. *Comput. Geosci.* 28, 929–937. doi: 10.1016/s0098-3004(02)00013-4

Perrot, Y., Brehmer, P., Roudaut, G., Gerstoft, P., and Josse, E. (2014). Efficient multibeam sonar calibration and performance evaluation. *Int. J. Eng. Sci. Innovat. Technol.* 3, 808–820.

Piñones, A., Hofmann, E. E., Dinniman, M. S., and Klinck, J. M. (2011). Lagrangian simulation of transport pathways and residence times along the western antarctic peninsula. *Deep Sea Res.* 58, 1524–1539. doi: 10.1016/j.dsr2.2010.07.001

Plagányi, ÉE., and Butterworth, D. S. (2012). The scotia sea krill fishery and its possible impacts on dependent predators: modeling localized depletion of prey. *Ecol. Appl.* 22, 748–761. doi: 10.1890/11-0441.1

Reid, K., and Brierley, A. S. (2001). The use of predator-derived krill length-frequency distributions to calculate krill target strength. *CCAMLR Sci.* 8, 155–163.

Reid, K., Watkins, J. L., Croxall, J. P., and Murphy, E. J. (1999). Krill population dynamics at south georgia 1991-1997, based on data from predators and nets. *MEPS* 177, 103–114. doi: 10.3354/meps177103

Reiss, C. R., Watters, G., Cutter, G., Cossio, A. M., and Walsh, J. (2021). Glider-based estimates of meso-zooplankton biomass density: a fisheries case study on antarctic krill (*Euphausia superba*) around the northern antarctic peninsula. *Front. Mar. Sci.* doi: 10.3389/fmars.2021.604043

Reiss, C. S., Cossio, A. M., Loeb, V., and Demer, D. A. (2008). Variations in the biomass of antarctic krill (*Euphausia superba*) around the South shetland islands, 1996–2006. *ICES J. Mar. Sci.* 65, 497–508. doi: 10.1093/icesjms/fsn033

Reiss, C. S., Hinke, J. T., and Watters, G. M. (2020). Demographic and maturity patterns of antarctic krill (*Euphausia superba*) in an overwintering hotspot. *Polar Biol.* 43, 1233–1245. doi: 10.1007/s00300-020-02704-4

Ressler, P. H., Robertis, A. D., Warren, J. D., Smith, J. N., and Kotwicki, S. (2012). Developing an acoustic survey of euphausiids to understand trophic interactions in the bering sea ecosystem. *Deep Sea Res. Part II Top. Stud. Oceanogr.* 65–70, 184–195. doi: 10.1016/j.dsr2.2012.02.015

Richerson, K., Watters, G. M., Santora, J., Shroeder, I. D., and Mangel, M. (2015). More than passive drifters: a stochastic dynamic model for the movement of antarctic krill. *Mar. Ecol. Prog. Ser.* 529, 35–48. doi: 10.3354/meps11324

Rudnick, D. L. (2016). Ocean research enabled by underwater gliders. *Ann. Rev. Mar. Sci.* 8:519. doi: 10.1146/annurev-marine-122414-033913

Siniff, D. B. (1991). An overview of the ecology of antarctic seals. *Amer. Zool.* 31, 143–149. doi: 10.1093/icb/31.1.143

Tapia, F. J., Pineda, J., Ocampo-Torres, F. J., Fuchs, H. L., Parnell, P. E., Montero, P., et al. (2004). High-frequency observations of wind-forced onshore transport at a coastal site in baja california. *Continental Shelf Res.* 24, 1573–1585. doi: 10.1016/j.csr.2004.03.013

Tarling, G. A., and Thorpe, S. E. (2014). Instantaneous movement of krill swarms in the antarctic circumpolar current. *Limnol. Oceanogr.* 59, 872–886. doi: 10.4319/lo.2014.59.3.0872

Testor, P., de Young, B., Rudnick, D. L., Glenn, S., Hayes, D., Lee, C. M., et al. (2019). OceanGliders: a component of the integrated GOOS. *Front. Mar. Sci.* 6:422. doi: 10.3389/fmars.2019.00422

Trenkel, V. M., and Berger, L. (2013). A fisheries acoustic multifrequency indicator to inform on large scale spatial patterns of aquatic pelagic ecosystems. *Ecol. Indic.* 30, 72–79. doi: 10.1016/j.ecolind.2013.02.006

Velasco, D. W., Nylund, S., and Pettersen, T. (2018). Combined current profiling and biological echosounding results from a single ADCP. *OCEANS MTS/IEEE* 2018, 1–5. doi: 10.1109/OCEANSKOBE.2018.8559356

Wall, C. C., Jech, J. M., and McLean, S. J. (2016). Increasing the accessibility of acoustic data through global access and imagery. *ICES J. Mar. Sci.* 73, 2093–2103. doi: 10.1093/icesjms/fsw014

Watkins, J. L., Reid, K., Ramm, D., Zhao, X. Y., Cox, M., Skaret, G., et al. (2016). The use of fishing vessels to provide acoustic data on the distribution and abundance of antarctic krill and other pelagic species. *Fish. Res.* 178, 93–100. doi: 10.1016/j.fishres.2015.07.013

Watters, G. M., Hinke, J. T., and Reiss, C. S. (2020). Long-term observations from antarctica demonstrate that mismatched scales of fisheries management and predator-prey interaction lead to erroneous conclusions about precaution. *Sci. Rep.* 10:2314. doi: 10.1038/s41598-020-59223-9

Wiebe, P. H., Ashjian, C., Lawson, G. L., Piñones, A., and Copley, N. (2011). Horizontal and vertical distribution of euphausiid species on the western antarctic peninsula southern ocean GLOBEC study site. *Deep Sea Res. II* 58, 1630–1651.

Woillez, M., Ressler, P. H., Wilson, C. D., and Horne, J. K. (2012). Multifrequency species classification of acoustic-trawl survey data using semi-supervised learning with class discovery. *J. Acoust. Soc. Am.* 131:685. doi: 10.1121/1.3678685

Zhou, M., and Dorland, R. D. (2004). Aggregation and vertical migration behavior of *Euphausia superba*. *Deep Sea Res. II* 51, 2119–2137.

Zhou, M., Nordhausen, W., and Huntley, M. (1994). ADCP measurements of the distribution and abundance of euphausiids near the antarctic peninsula in winter. *Deep Sea Res. Part I Oceanogr. Res. Papers* 41, 1425–1445. doi: 10.1016/0967-0637(94)90106-6

Conflict of Interest: SN was employed by the company Nortek Group.

The remaining authors declare that the research was conducted in the absence of any commercial or financial relationships that could be construed as a potential conflict of interest.